Altitudinal variation in impacts of snow cover, reservoirs and precipitation seasonality on monthly runoff in Tibetan Plateau catchments

Nan Wu^{a,b,c,f}, Ke Zhang^{a,b,c,d,e,*}, Amir Naghibi^f, Hossein Hashemi^f, Zhongrui Ning^{b,c}, Jerker Jarsjö^g

^aThe National Key Laboratory of Water Disaster Prevention, Hohai University, Nanjing, Jiangsu, 210024,

5 China

^bYangtze Institute for Conservation and Development, Hohai University, Nanjing, Jiangsu, 210024, China
^cCollege of Hydrology and Water Resources, Hohai University, Nanjing, Jiangsu, 210024, China
^dChina Meteorological Administration Hydro-Meteorology Key Laboratory, Hohai University, Nanjing, Jiangsu, 210024, China

10 "Key Laboratory of Water Big Data Technology of Ministry of Water Resources, Hohai University, Nanjing, Jiangsu, 210024, China

^fDivision of Water Resources Engineering, LTH, Lund University, Lund, 22100, Sweden ^gDepartment of Physical Geography, Stockholm University, Stockholm, 10691, Sweden;

15 Nanjing, Jiangsu, 210098, China

E-mail address: kzhang@hhu.edu.cn (Ke Zhang)

^{*} Corresponding author at: The National Key Laboratory of Water Disaster Prevention, Hohai University,

ABSTRACT

20

25

30

35

Understanding monthly runoff variability, its spatio-temporal characteristics, and key drivers under climate change and human impacts is crucial for long-term water resource management. However, current knowledge remains limited, especially in high-elevation, seasonally cold regions. Focusing on 10 sub-basins along an elevation gradient (1000 to 5900 m a.s.l.) in the hydrologically complex Yalong River basin, China, this study developed an extended Budyko framework based on monthly water balances (2002–2016), explicitly separating snow storage dynamics (ΔS_{snow}) from other terrestrial water storage changes (ΔS '), including those related to hydropower reservoir construction. Results showed that snow accumulation and snowmelt are main drivers of runoff seasonality in the upper sub-catchments, and their effects propagate to the lower-elevation snowfree sub-catchments, which are also subject to additional influence from hydropower reservoirs. This created pronounced altitudinal heterogeneity in drivers of monthly runoff, a phenomenon suggested but rarely quantified at high spatio-temporal resolution in other global regions. Furthermore, a decrease in runoff seasonality in the Yalong River at its Yangtze River outlet (that receives water from all 10 investigated sub-basins) was observed, this change appeared unrelated to snow storage changes and was more likely driven, by trends in unfrozen precipitation seasonality and/or flow-modulating impacts of reservoirs, natural lakes and groundwater. Future snow thinning may exacerbate these trends. Implementing the variance decomposition method within the extended Budyko framework, the intra-annual runoff variability $(\sigma^2 R)$ was captured by calculating the variance and covariance of influencing factors, achieving R² values above 0.9 in most sub-basins, and the rainfall (P_r) and ΔS variances were identified as the main contributors. Methodologically, we have verified the substantial contribution of hydropower reservoir storage changes on total storage changes by independent analysis of reservoir storage data. These findings

effective water resource allocation, current knowledge of monthly runoff variability, its spatio-temporal characteristics. and underlying key drivers, including their sensitivity to climate change and other human impacts, is limited. With a particular focus on 10 sub-basins along an elevation gradient (1000 to 5900 m.a.s.l.) in the hydrologically complex, seasonally cold Yalong River basin, China, this study developed an extended Budyko framework based on monthly water balances (2002-2016) to consider snow storage dynamics (ΔS_{snow}) separately from other terrestrial water storage changes (ΔS '), including those related to hydropower reservoir construction. Results showed that snow accumulation and snowmelt are main drivers of runoff seasonality in the upper sub-catchments of the Yalong River basin, with propagating impacts also on lower-elevation snow-free sub-catchments, which are increasingly under the additional influence of hydropower reservoirs. This creates a relatively strong altitudinal heterogeneity in drivers of monthly runoff, which has been hypothesized to occur also in other world regions including e.g. major European rivers of Alpine origin, although not yet quantified at similarly high spatio-temporal resolution.

Deleted: Although of great importance for long-term,

Deleted: an observed

Deleted: shown

Deleted: to be

Deleted: hence likely caused

Deleted: constructed

Deleted:

 $\textbf{Deleted:} \ implying \ that \ f$

Deleted: urther snow thinning may exacerbate such trends in the future

Deleted: based on

Deleted: (

Deleted:)

Deleted: with the main contributors being variances of rainfall (P_r) and $\Delta S'$.

Deleted:,

Deleted: supporting

supported the applicability of the extended monthly Budyko framework for identifying dominant processes in the context of runoff generation and the rapid environmental changes that the Yalong River basin and other cold regions (not least of the Tibetan plateau) are currently experiencing.

Keywords: Runoff variability, Snowmelt, Terrestrial storage change, Altitudinal trend, Correlation analysis, Budyko framework, Yalong River basin

1. Introduction

80

85

90

95

100

Runoff is a key component of the hydrological cycle and is highly susceptible to external environmental factors, primarily climate change and human activities, which can lead to significant changes in hydrological processes (Bao et al., 2023). Climate variations such as precipitation intensity, rising temperature, and enhanced radiation not only affect the water vapor content in the atmosphere but also alter the surface characteristics of catchments (Li and Quiring, 2021). Moreover, extensive human activities such as reservoir construction increase the complexity of surface water flow, making accurate analysis of the hydrological cycle a challenge (Gutenson et al., 2020). Observations indicate that 24% of the global river flow has undergone significant changes (Li et al., 2020). Runoff changes, influenced by evolving factors (Yao et al., 2020), show the sensitivity of hydrological cycles to climate conditions and surface characteristics (Huang et al., 2021). While intra-annual analysis of runoff response to climate variability and change provides vital information for the effective allocation of water resources, a significant amount of research is focused on multi-annual timescale analysis (Huo et al., 2021; Ning et al., 2017; Tu et al., 2015). Changes in monthly climate conditions and human activities largely drive variations in monthly runoff (Xin et al., 2019; Yao et al., 2020).

In many parts of the world, seasonal storage of snow and ice provides meltwater and secures water supply over the growing season_(Qi et al., 2019). Although climate change impacts

Formatted: Font color: Blue

frequently act to reduce seasonal volumes of stored snow and ice, it is challenging to predict the consequences for runoff. This is partly due to the difficulty of disentangling such impacts from other influences on runoff, such as changes in precipitation and temperature, and reservoir construction (Gan et al., 2022). Benchmark estimates have shown that that snowmelt during the rainy season (April to June) contributed to 31% of the annual runoff for the source regions of the Indus River, while the source regions of the Yellow River, Yangtze River, Mekong River, Thanlwin River, and Brahmaputra River received snowmelt from April to June, contributing to 20-23% of the annual runoff (Zhang et al., 2013). Additionally, the snowfall-to-precipitation ratio has been found to exert a significant influence on both annual runoff and intra-annual runoff variation (Berghuijs et al., 2014; Liu et al., 2022; Zhang et al., 2015).

110

115

120

Recent studies on this topic have also shown evidence of decreased runoff seasonality, e.g. in snow-dominated rivers of central Europe (Rottler et al., 2020). In cold regions of China, water storage and runoff characteristics show quite complex spatio-temporal patterns over the last 30 years (Fang et al., 2019). This is particularly the case in the downstream regions that use reservoirs to alter the intra-annual hydrological cycle and store water to ensure a sustainable water supply during dry seasons in the face of agricultural, industrial, and domestic demands (Shen, 2018). More generally, water storage in lakes, reservoirs and groundwater aquifers may contribute considerably to monthly runoff dynamics (Bai et al., 2018; Hwang and Devineni, 2022; Shi and Gao, 2022). It is hence most likely that distinct differences in drivers of monthly runoff exist across altitudinal gradients of different mountainous regions of the world (Kuhn et al., 2016; Rottler et al., 2020; Shen, 2018), although the details of such patterns are largely unexplored. Zhang et al. (Zhang et al., 2016) emphasized that main factors (e.g., human activities and climate-driven changes in runoff) that affect the runoff variance deserve more attention. A more detailed

Formatted: Font color: Blue

understanding of intra-annual runoff characteristics in mountainous watersheds under changing environments combined with attribution analyses are crucial for sustainable water resource management (Dethier et al., 2020; Liu et al., 2017).

125

130

135

140

145

Precipitation and potential evapotranspiration define catchment water availability and storage capacity (Huang et al., 2021; Li et al., 2021; Yao et al., 2020). On a multi-year scale, precipitation is partitioned into evapotranspiration and runoff, reflecting competition between water supply (precipitation) and available energy (potential evapotranspiration) and regulated by the corresponding underlying surface characteristics (Wu et al., 2018). To analyze annual and multi-year scale hydrological processes considering rainfall and runoff changes, the Budyko framework has been widely used (Choudhury, 1999). The framework was initially developed to address water resource constraints through multi-year averages (Kazemi et al., 2021; Wang and Tang, 2014; Yang et al., 2008; Zhang et al., 2004) and has been widely applied to quantitatively analyze the impact of climate change and human activity on runoff (Liu et al., 2021; Wang and Tang, 2014; Xu et al., 2014). However, since this framework assumes multi-year, steady-state conditions, it is not applicable at intra-annual timescales. Furthermore, most assessments investigate the main drivers only by comparing runoff sensitivity, rather than their relative contribution to the actual variance of runoff (Liu et al., 2019).

Recently, some studies have attempted to extend the Budyko framework to intra-annual timescales, mainly by including monthly terrestrial water storage changes as part of the water supply (Du et al., 2016; Liu et al., 2019) and establishing a new water supply-demand relationship on monthly scale (Huang et al., 2021; Wu et al., 2019). Other studies have also integrated monthly terrestrial water storage in water balance using the Budyko framework along with hydrological models (Yao et al., 2020; Zhang et al., 2020). Some studies have demonstrated that incorporating

terrestrial water storage significantly enhances predictability compared to the previous precipitation and potential evapotranspiration relationship (Wu et al., 2018; Zhang et al., 2010). Although the extended Budyko framework has been effective to analyze monthly runoff changes, the attribution analysis of intra-annual runoff changes needs to consider more driving factors, particularly due to the complexity and interaction of climate change and human activities in the cold mountainous regions (Liu et al., 2018; Luo and Lau, 2018). Equally important from a process understanding perspective is the consideration of sufficiently fine-resolved temporal and spatial scales (Fang et al., 2016).

150

155

160

170

The Qinghai-Tibet Plateau, often referred to as the "Third Pole," is a region where the atmosphere, hydrosphere, cryosphere, and biosphere intricately interact (Bao et al., 2023; Cui et al., 2023). Snow accumulation begins in the fall, lasting until the subsequent spring, and in some high-altitude areas, snow cover persists even into the summer months (Wang et al., 2018; Wu et al., 2012). Snowmelt runoff stands as a crucial component of the primary runoff source on the Qinghai-Tibet Plateau, exhibiting distinct seasonal variations and primarily impacting spring runoff (Gao et al., 2017; Han et al., 2019).

We here consider the Yalong River basin, situated between 1000 and 5900 m.a.s.l. in the southeastern part of the Tibetan Plateau, which experiences seasonal snow cover in its upstream regions (with few glaciers, which can be ignored (Qi et al., 2022)), while the construction of downstream cascade hydropower stations has greatly affected terrestrial water storage capacity. These factors exert significant influences on regional water cycling, especially at the intra-annual scales (Wang et al., 2018; Wu and Shen, 2007). Therefore, this study aims to (1) extend the Budyko framework to distinguish between snow storage change (ΔS_{snow}) and remaining water storage change ($\Delta S'$) in monthly water balances; (2) determine interannual and intra-annual

variations of hydrological variables including runoff (R), rainfall (P_r) , snowmelt (S_{melt}) , evapotranspiration (E) and terrestrial water storage change (ΔS) in nested catchments along a pronounced altitudinal gradient, and (3) examine how relationships between runoff and other factors can vary with elevation, including assessments of major contributors to runoff variation (using variance decomposition analysis); and (4) discuss wider implications including the susceptibility of the identified monthly runoff contributors to climate-change and other human impacts.

2. Methods and application

In this section, the representative study area and the required data for this study are introduced in Sect. 2.1, while the theoretical framework for attributing runoff variability based on the extended Budyko is described in Sect. 2.2. Table 1 presents the variables and acronyms used in this study.

Table 1. Description of hydrological variables and acronyms.

Number	Variable (mm)	Abbreviation			
1	Precipitation	P			
2	Rainfall component of P	mponent of P P_r			
3	Snowfall component of P P_s				
4	Total available water P'				
5	Potential evapotranspiration E_{θ}				
6	Actual evapotranspiration E				
7	Runoff	R			
8	Change in terrestrial water storage	ΔS			
9	Change in ground snowpack storage	ΔS_{snow}			
10	Differences between ΔS and ΔS_{snow}	$\Delta S' = \Delta S - \Delta S_{snow}$			
11	Snow melt	S_{melt}			

2.1. Study area and data

2.1.1. Study area

The Yalong River is the largest tributary of the Jinsha River, which forms the upper reaches

Deleted: 1

Deleted: Then, the implementation of the extended Budyko framework is explained in Sect. 2.2.

175

of the Yangtze River. Encompassing a wide range of altitudes (1,000–5,900 m a.s.l.) and hydroclimatic conditions, and increasingly impacted by human activities such as hydropower development, the Yalong River basin serves as an ideal case study to test our method. It flows from northwest to southeast, with a total length of 1,570 km and a drainage area of 128,000 km². Due to the complex topography, meteorological observations in the upper reaches are limited (Fig. 1). Precipitation and temperature generally increase from north to south, with summer temperatures ranging from -3 °C in the north to 26 °C in the south, and winter temperatures from -18 °C to 14 °C. Annual precipitation ranges from 600–800 mm in the upper region, 1,000–1,400 mm in the middle region, and 900–1,300 mm in the lower region. The rainy season occurs from June to October. The annual average discharge at the confluence with the Yangtze River is 1,900 m³/s, with a total annual runoff of nearly 60 billion m³, accounting for 13% of the upstream flow of the Yangtze River (He et al., 2015).

190

195

200

205

210

The Yalong River is renowned for its abundant hydropower resources. The middle and lower reaches have been designated as a national hydropower base, ranking third among the 13 major hydropower bases in China (Wu and Shen, 2007). In the downstream section, the construction of five major hydropower stations — including Jinping I (2013), Jinping II (2013), Guandi (2012), Ertan (1999), and Tongzilin (2015) — has significantly altered terrestrial water storage and flow regimes (Wu and Shen, 2007).

To assess the spatially varying impacts of hydropower regulation on runoff seasonality, the Yalong River basin was divided into ten sub-basins, forming a nested catchment structure. The upstream sub-basins, located in high-altitude regions, are primarily influenced by seasonal snow accumulation and melt, while glaciers are sparse and thus negligible. These areas experience limited human interference, serving as relatively natural or minimally disturbed reference

catchments. In contrast, the downstream sub-basins are heavily regulated by cascade hydropower operations, which have significantly modified water storage dynamics and streamflow patterns. This upstream—downstream contrast enables a comparative analysis of natural versus regulated runoff responses within the Budyko framework. The sub-basins were delineated based on the distribution of hydrological stations (Fig. 1), and the coordinates and basic hydrological and meteorological characteristics of each sub-basin are listed in Table 2.

Formatted: Border: Bottom: (No border)

Formatted Table

Table 2. Location of outlet stations in 10 sub-basins and basic hydrological and meteorological information.

218

219

Number	Site Name	Elevation (m)	<u>Latitude</u>	Longitude	Area (million km²)	Monthly Streamflow (mm)	Monthly Precipitation (mm)	$\frac{\text{Monthly}}{\text{Temperatures}}$ $\frac{(^{\circ}C)}{}$	Monthly Potential Evapotranspiration (mm)
1	Ganzi (GZ)	<u>3360</u>	31.62°	99.97°	3.27	21.45	<u>54.74</u>	<u>-1.60</u>	61.25
<u>2</u>	Zhuba (ZB)	3391	31.43°	100.68°	0.69	24.28	63.63	<u>-0.45</u>	<u>62.75</u>
<u>3</u>	Daofu (DF)	<u>3159</u>	31.03°	101.07°	0.73	28.88	66.22	0.73	66.69
<u>4</u>	Yajiang (YJ)	<u>2714</u>	30.03°	101.02°	1.89	40.96	70.92	2.18	<u>73.47</u>
<u>5</u>	Zhuosang (ZS)	<u>3652</u>	<u>29.70°</u>	100.38°	<u>0.31</u>	40.95	<u>68.30</u>	1.77	<u>76.10</u>
<u>6</u>	Luning (LN)	<u>1680</u>	<u>28.45°</u>	<u>101.87°</u>	<u>3.64</u>	<u>38.73</u>	80.87	<u>5.95</u>	81.93
<u>7</u>	Wulaxi (WLX)	<u>4067</u>	28.48°	<u>101.65°</u>	0.25	40.66	92.78	3.13	<u>72.96</u>
<u>8</u>	Lugu (LG)	<u>1621</u>	28.30°	<u>102.18°</u>	0.21	84.13	<u>97.20</u>	<u>8.65</u>	<u>78.73</u>
<u>9</u>	Sunshuiguan (SSG)	<u>1705</u>	28.30°	<u>102.20°</u>	<u>0.16</u>	55.74	94.93	10.25	<u>81.66.</u>
<u>10</u>	Tongzilin (TZL)	<u>1081</u>	26.68°	<u>101.85°</u>	1.65	<u>62.31</u>	91.58	13.29	99.47

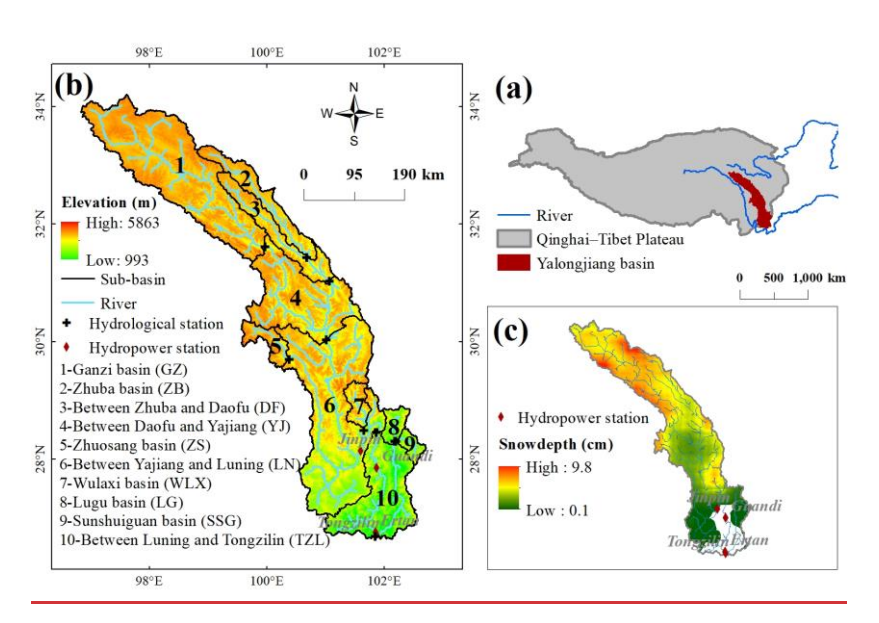


Figure 1. (a) Geographic locations, (b) elevation of the 10 sub-basins (based on data from the U.S. Geological Survey), and (c) mean annual snow depth (based on data from the National Tibetan Plateau Data Center) for the period 2002-2016 in the Yalong River basin.

2.1.2. *Dataset*

220

225

230

The average monthly runoff records during the period 2002-2016 at 10 hydrometry stations were obtained from the China Hydrological Yearbook provided by the Ministry of Water Resources of China. This period was chosen because it represents the timeframe during which consistent runoff data were available for all ten sub-basins. Moreover, this period enables an assessment of the impacts of reservoir construction and operation on the hydrological processes in the region. Table 2 gives information about the locations of stations and their corresponding sub-basins, including runoff, precipitation, temperature, and potential evapotranspiration. The first column represents the labels of the 10 sub-basins, as depicted in Fig. 1, with the Tongzilin Hydrological Station serving as the controlling station for the entire Yalong River basin.

Formatted: Centered

Deleted: (1-10)

Formatted: Font: 10.5 pt

Formatted: Font: 10.5 pt

For meteorological data, the CN05.1 dataset (1961-2020) was utilized in this study, which provides a daily grid resolution of 0.25°×0.25°, covering various meteorological variables, including precipitation, temperature, atmospheric pressure, relative humidity, sunshine hours, and wind speed across China. The dataset has been generated by interpolation of data from over 2,400 observation stations throughout China using the "abnormal method" (New et al., 2000). Digital Elevation Model data at a 1km resolution were sourced from the U.S. Geological Survey (USGS) (GTOPO30, http://edc.usgs.gov/products/elevation/gtopo30/gtopo30.html). This study used a dataset of the spatial distribution of degree-day factors for glaciers and snow in High Mountain Asia, which was derived from observations over 40 glaciers. The spatial resolution of this dataset is 0.5°, with units of mm/°C/day (Zhang et al., 2019). The evapotranspiration data was derived from GLEAM (Global Land-surface Evaporation: the Amsterdam Methodology) (1980-2020), which combines a wide range of remote sensing observations to derive daily actual evapotranspiration and its different components, including snow sublimation (Miralles et al., 2011).

2.2. Methods

240

245

250

255

Fig. 2 provides an overview of the workflow applied in this study, summarizing the extended Budyko calculations and the subsequent statistical analyses, which are organized into three main parts. Part 1 corresponds to the estimation of monthly water balance components across the ten sub-basins of the Yalong River basin using observed temperature (*T*), precipitation (*P*), and runoff (*R*) data. These calculations follow the extended Budyko framework introduced in Sect. 2.2.1, and the derived hydrological variables are listed in Table 1. In addition to two relatively large headwater catchments and four smaller ones, four nested catchment areas were also considered (see Sect. 2.1.1 for details). For each nested catchment, the net runoff (*R*) at a given time was calculated as the difference in measured discharges

Deleted: 1

Deleted: Figure

Deleted: Fig. 1 2 provides an overview of the extended Budyko calculation used in thisfor the present study

Formatted: Font: Italic

Formatted: Font: Italic

Formatted: Font: Italic

Deleted: Observation data on temperature T, precipitation P and runoff R were used to resolve monthly water balances, and for estimatione of multiple hydrological variables (included listed in Table 1) in across ten sub-basins of the Yalong River basin.

Deleted: we here consider four nested catchment areas

Deleted: further the study area description of

Deleted: 2

 $(\Delta O = O_{down} - O_{up})$ between the downstream and upstream gauging stations, divided by the <u>difference in catchment areas</u> ($\Delta A = A_{down} - A_{up}$). For the headwater catchments, Q_{up} and A_{up} are per definition equal to zero. Part 2 involves exploring the statistical relationships between R and the hydrological variables (including potential drivers of R, such as P_r , S_{melt} , ΔS , and E; Table 1). This analysis focuses particularly on identifying any lag times in the runoff response to precipitation events and is described in Sect. 2.2.2. Part 3 consists of quantifying the relative contributions of different driving factors to monthly runoff variability through a variance decomposition approach, as explained in Sect. 2.2.3. Together, these three parts provide a comprehensive framework for investigating the processes that control intra-annual runoff variability in the Yalong River basin. All hydrological variables used in this study are summarized in Table 1.

275

280

285

290

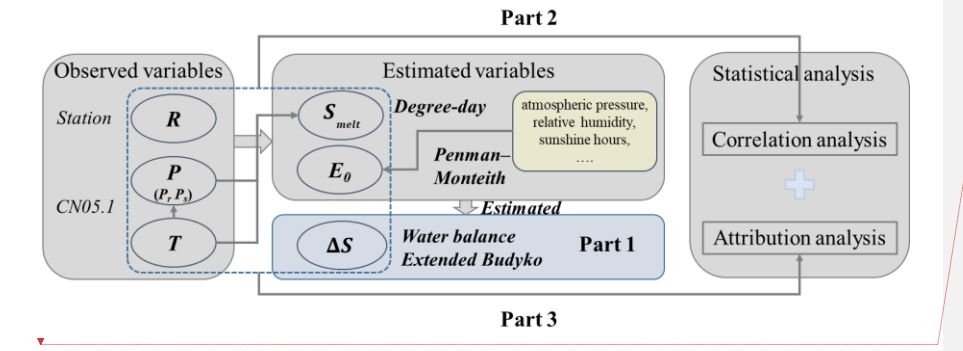


Figure 2. Flowchart of the extended Budyko framework. Italic text represents the data source, and italicbold text represents the calculation method for obtaining the data.

2.2, 1 Extended Budyko framework by decomposing ΔS

coupling theory, which, compared with statistical empirical methods, offers clearer physical meaning and is easier to calculate and parameterize (Hwang and Devineni, 2022; Shi and Gao, 2022). The partitioning of annual precipitation into evapotranspiration and runoff is governed

The present analyses use water balance methods based on the Budyko hydrothermal

Deleted: for which the net runoff R at any particular time is quantified as the difference in measured discharges $\Delta Q = Q_{down} - Q_{up}$ between the downstream discharge station and upstream discharge station, divided by the corresponding difference in catchment areas $\Delta A = A_{down} - A_{up}$.

Formatted: Font: Italic

Formatted: Font: Italic

Deleted: The water balance variables were then used as input to an extended Budyko framework. Subsequently, the correlation between monthly R and the hydrological variables (including drivers of R, such as P_r , S_{melt} , ΔS , and E; Table 1) was explored, focusing on the lag time of R response to Pevents. Finally, the relative contributions of driving factors to monthly runoff variability were quantitatively assessed using the variance decomposition method. The hydrological variables employed in this study are shown in Table 1.

Deleted: 1

Deleted: 1

Deleted: possesses substantial physical significance

Deleted: straightforward

Deleted: annual

Deleted: streamflow

by the balance between available water and energy (Huang et al., 2021), and several empirical equations have been developed to characterize this relationship, (Choudhury, 1999; Wang and Tang, 2014; Yang et al., 2008; Zhang et al., 2004), We consider one of the most popular equations, namely Choudhury-Yang:

$$E = \frac{P \times E_0}{(P^n + E_0^{\ n})^{1/n}} \tag{1}$$

where potential evapotranspiration (E_{θ} , mm) and precipitation (P, mm) act as indicators for energy and water supply, respectively, and where E (mm) is the calculated actual evapotranspiration, and n is a landscape parameter, mainly expressing impacts of prevailing surface conditions within the basin.

315

320

325

The water balance equation on the decadal time scale for a basin can be expressed using equation (2), wherein P represents the total water input to the basin. The outputs comprise runoff (R, mm) and evapotranspiration (E, mm).

$$P = R + E \tag{2}$$

The change in terrestrial water storage can be assumed to be approximately 0 on the decadal time scale, while on the intra-annual time scale, it cannot be neglected (Huang et al., 2021; Xu et al., 2012):

$$P = R + E + \Delta S \tag{3}$$

In order to consider the dynamic changes of monthly snow accumulation and melting separately, P was differentiated into rainfall (P_r , mm) and snowfall (P_s , mm) using daily temperature thresholds (Widen-Nilsson et al., 2007), and the terrestrial water storage change was also divided into two components: one accounts for snow storage change (ΔS_{snow} , mm), and the other represents the remaining storage changes ($\Delta S'$ mm; mainly including storage 330 changes in surface water, groundwater and soil water). Thus, Equation (3) can be expressed as:

$$P_r + P_s = R + E + \Delta S_{snow} + \Delta S' \tag{4}$$

In this study, the cumulative value of daily P_r (and P_s) was calculated based on daily

Deleted: determined by the competition between available water and available energy measured by potential evapotranspiration

Deleted: many scholars have proposed

Deleted: that is a part of the Budyko framework

Deleted: However, due to their simplicity and effectiveness, some of those equations have been applied more than others

temperature to derive monthly P_r (and P_s). ΔS_{snow} is mainly supplied in solid form by P_s and depleted in liquid form by melting snow (S_{melt} , mm). Equation (4) can then be expressed as:

$$P_r + P_S = R + E + (P_S - S_{melt}) + \Delta S'$$
(5)

The monthly water balance equation can be written as:

340

345

350

355

$$P_r + S_{melt} = R + E + \Delta S' \tag{6}$$

Therefore, the total available water (P') for E and R is expressed as the sum of P_r , S_{melt} and $\Delta S'$ (Zeng and Cai, 2015). Accordingly, Equation (6) can be modified as follows:

$$P' = P_r + S_{melt} - \Delta S' = R + E \tag{7}$$

Combining equation (1) and equation (7), an extended Budyko framework with a parameter n can be formulated as:

$$E = \frac{(P_r + S_{melt} - \Delta S') \times E_0}{((P_r + S_{melt} - \Delta S')^n + E_0^n)^{1/n}}$$
(8)

In this study, the Penman-Monteith method (Allen et al., 1998) was used for E_{θ} calculation. Consistent with the FAO Irrigation and Drainage Paper No. 56, the Penman-Monteith method is recognized as a physically based and reliable approach for estimating E_{θ} , and is often used as a benchmark for evaluating empirical methods (Chen et al., 2005). It has also been widely applied to estimate evapotranspiration from snow surfaces (Stigter et al., 2018; Xin et al., 2021), considering it a saturated or unstressed surface similar to water surfaces (Yang and Bai, 2023). Due to the high albedo of snow surface, the outgoing radiation is often greater than the incoming radiation, leading to negative net radiation in many snow-covered areas. Since the evaporation mechanisms under negative net radiation condition are still not well understood. E is assumed to be 0 when the net radiation is less than 0, following Gan et al. (2022).

Therefore, the monthly runoff R can be expressed as:

$$R = P_r + S_{melt} - \Delta S' - \frac{(P_r + S_{melt} - \Delta S') \times E_0}{((P_r + S_{melt} - \Delta S')^n + E_0^n)^{1/n}}$$
(9)

in which R was obtained from direct discharge measurements, and Smelt was computed

Deleted:

Deleted: e.g. in consistency with the

Deleted: (Allen et al., 1998) showing that the Penman-Monteith model is a preferable physical approach to estimate

Formatted: Font color: Auto

Deleted: is often utilized as a standard method for verifying other empirical methods

Deleted: The Penman-Monteith method

Deleted: employed for estimating evapotranspiration on snow surfaces

Formatted: Font color: Auto

Deleted: the surface radiance is typically higher than that of the air, resulting in negative net radiation for many snow-covered pixels

Deleted: Currently,

Deleted: s

Deleted: is

Deleted: under-studied

Deleted:

Deleted: Therefore, in this study,

Deleted:

Deleted:

Deleted:

380

385

390

395

400

using the degree-day method. The n parameter is primarily employed to characterize the underlying surface conditions, including factors such as average slope (Zhang et al., 2004) and vegetation type or land use (Bounoua et al., 2004). Although n may vary over long-term scales due to landscape changes, it typically remains stable at shorter, monthly timescales. Therefore, following Huang et al. (2021), we assumed that n can be treated as constant value for monthly scales. We hypothesized and tested our assumption, n, by calculating the evapotranspiration using the Budyko and extended Budyko. As shown in Table S1, the results demonstrated a high correlation coefficient between the two models, supporting our assumption of a constant n. Based on this, the monthly $\Delta S'$ was calculated by closing the water balance.

The degree-day method was adopted for S_{melt} estimation as it requires only readily available temperature data and straightforward calculations, while offering comparable accuracy to the energy balance method at the basin scale (Hock, 2003). This method assumes a strong positive linear relationship between temperature and snowmelt. The fundamental equation, presented as equation (10), states that if the daily temperature (T_i) exceeds a threshold temperature (T_0), the S_{melt} is determined by the degree-day factor (D_i , mm/°C/day) and temperature;

$$S_{melt} = D \times (T_i - T_0) \qquad if T_i > T_0$$
 (10)

In this method, the parameter D typically falls within the range of 2.5-14 mm/°C/day, with specific values described in Sect. 2.2.2. T_{θ} is commonly assumed to be 0°C, and S_{melt} is constrained by the presence of existing snow depth.

2.2,2. Cross correlation analysis

Runoff is influenced by various natural and geographical factors. To further examine the relationships between R and individual hydrological drivers (such as P_r , S_{melt} , ΔS , E), we applied partial correlation analysis, which allows us to control for the effects of other variables. Before performing these correlation analyses, all time series were detrended to minimize the

Deleted: of the basin

Deleted: (Bounoua et al., 2004),

Formatted: Font: Italic

Deleted: which might undergo significant changes on longterm scales, whereas differences over short-term scales, such as monthly, are typically minimal.

Deleted: based on a previous study

Deleted: (

Formatted: Font color: Auto

Deleted: and multi-year

Deleted: showed

Deleted: evapotranspiration values in both

Deleted: which supports our hypothesis.

Deleted: Thus,

Deleted: relies on readily available data and straightforward calculations, providing comparable accuracy to the energy balance method at the basin scale (Hock, 2003). The degreeday model operates on the assumption of a strong positive linear correlation between temperature and S_{melt} , with the fundamental equation depicted in equation (10). If the daily temperature T_i surpasses the temperature threshold T_{0} , the S_{melt} is determined by the degree-day factor $(D, \, \text{mm})^{\circ}\text{C}/\text{day})$ and temperature:

Deleted: 1

Formatted: Font: Italic

influence of long-term trends that could otherwise bias the estimated relationships (Wu et al., 2024). This approach helps to isolate the independent contribution of each variable to runoff variability, reducing confounding effects from other hydrological processes.

In addition, because runoff responses in the basin tend to become smoothed and delayed after undergoing complex surface and subsurface hydrological processes (Brutsaert and Hiyama, 2012), we introduced the variable τ to characterize the lag time between monthly precipitation events and corresponding runoff responses in the Yalong River basin. τ was calculated within a range of 0 to 5 months, with statistical significance assessed at a threshold of $p \le 0.05$.

430

440

2.2,3. Quantifying the contributions of different factors to runoff variability

Equation (9) could be expressed as $R = f(P_r, S_{melt}, \Delta S', E_{\theta})$. The variance of R (within a year) is determined by the variance of each driving factor $(P_r, S_{melt}, \Delta S', E_{\theta})$ and their covariance (Ye et al., 2015):

$$\sigma_{R}^{2} = \left(\frac{\partial f}{\partial P_{r}}\right)^{2} \sigma_{P_{r}}^{2} + \left(\frac{\partial f}{\partial S_{melt}}\right)^{2} \sigma_{S_{melt}}^{2} + \left(\frac{\partial f}{\partial \Delta S'}\right)^{2} \sigma_{\partial \Delta S'}^{2} + \left(\frac{\partial f}{\partial E_{0}}\right)^{2} \sigma_{E_{0}}^{2} + 2\left(\frac{\partial f}{\partial P_{r}}\right)^{2} \left(\frac{\partial f}{\partial S_{melt}}\right)^{2} \left(\frac{\partial f}{\partial S_{melt}}\right)^{2} \left(\frac{\partial f}{\partial P_{r}}\right)^{2} \left(\frac{\partial f}{\partial S_{melt}}\right)^{2} \left(\frac{\partial f}{\partial P_{r}}\right)^{2} \left(\frac{\partial f}{\partial P_{r}}\right)^{2} \left(\frac{\partial f}{\partial P_{r}}\right)^{2} \left(\frac{\partial f}{\partial S_{melt}}\right)^{2} \left(\frac{\partial f}{\partial S_{mel$$

Hence, equations (11) are utilized to compute the contributions of the variance of each driving factor (P_r , S_{melt} , $\Delta S'$, E_{θ}) and their covariance to intra-annual runoff variability for the period 2002-2016.

Formatted: Font color: Blue

Deleted: Runoff is influenced by a variety of natural and geographical factors, with precipitation serving as the primary driver.Runoff is influenced by various natural and geographical factors, such as climate and the underlying surface. Precipitation serves as the primary driving factor in the formation of runoff. After undergoingFollowing complexintricate surface and subsurface hydrological processes, the catchment responses to precipitation tends to become smoothed and delayedgradually undergoes smoothing and lagging (Brutsaert and Hiyama, 2012). To characterize the hysteresis relationship between monthly precipitation and runoff in the Yalong River basin,the hysteresis relationship between monthly precipitation and runoff within Yalong River basin, we introduced the variable the variable τ , representing the lag time between precipitation events and corresponding runoff responses.to compute the lag time between the precipitation events and subsequent runoff changes, τ was calculated within a range of ranging from 0 to 5 months. Statistical significance was assessed considered at a threshold of as $p \le 0.05$ for this analysis.¶

Deleted: 1

Deleted: 10

465 **3. Results**

475

480

485

3.1. Intra-annual changes in hydrological variables

Fig. 3 depicts the full time series of P_r , S_{melt} , E, R, ΔS_{snow} , and ΔS of 10 sub-basins within the Yalong River basin from 2002 to 2016. It should be noted that R refers to the net runoff generated locally within the sub-basin, which in case of nested basins (DF, YJ, LN and TZL) excludes flows generated by areas further upstream. Fig. 3 shows that P_r exhibited pronounced interannual variation and was additionally higher in downstream areas. Smelt and \(\Delta Ssnow primarily occurred in the middle and upper reaches, including upstream sub-basins such as GZ, ZB, DF and YJ (Fig. 3). Lower reaches subbasins with $\Delta S_{snow} = 0$ (WLX, LG, SSG, TZL) would hence per definition have $\Delta S = \Delta S'(\Delta S > 0)$ means storage water, otherwise release). Within upstream areas E approached zero in the winter. Notably, the R and ΔS in WLX underwent an abrupt change in 2009, demonstrating a significant decrease in R and general increases in ΔS . The R decrease may in part be caused by filling of reservoirs and reservoirinduced increases in ΔS . In LN, the R and ΔS began to change around 2013, with locally created R fluctuating gently and ΔS starting to show pronounced intra-annual fluctuations including considerably higher positive values, which is consistent with the construction period of the Jinping hydropower station including the filling of the dam and the start of intra-annual flow regulations. In the upstream sub-basins unaffected by reservoir regulation, long-term ΔS values fluctuated around zero, suggesting that the hydrological system remained balanced under natural conditions. In contrast, the downstream sub-basins influenced by reservoir operations (e.g., WLX, LG, TZL) exhibited larger and more frequent fluctuations in ΔS, predominantly negative. This pattern was likely due to the cumulative effects of long-term reservoir regulation in the study area. Additionally, the periodic characteristics of R (more runoff in summer and less in winter) in lower elevation regions of LG and TZL were not as clear as in other regions,

Deleted: 2.2. Study area and data¶

2.2.1. Study area¶

The Yalong River is the largest tributary of the Jinsha River, which is made up of the upper reaches of the Yangtze River. Being a basin that encompasses a wide range of altitudes (1,000 to 5,900 m.a.s.l.) and hydro-climatic conditions (see below) while being increasingly impacted by human activities including hydropower expansion, it serves as a case study to test our method. It traverses from northwest to southeast. boasting a total length of 1,570 km and a drainage basin area of 128,000 km2. Meteorological observations in the upper reaches of the basin are limited due to the complex topography (Fig. 2). The precipitation and temperature in the Yalong River basin increases from north to south, with an average annual temperature of -3 in the north to 26 °C in the south in summer and -18 in the north to 14 °C in the south in winter. The precipitation ranges from 600 to 800 mm in the upper region, 1,000 to 1,400mm in the middle region, and 900 to 1,300 mm in the lower region. June to October is the rainy season. The annual average discharge at its confluence with the Yangtze River is 1,900 m³/s, with an annual discharge of nearly 60 billion m3, representing 13% of the total water volume upstream of the Yangtze River (He et al., 2015). ¶

hydropower resources and the middle and lower reaches are designated to the national hydropower base, ranking third among the 13 hydropower bases in China (Wu and Shen, 2007). In the downstream reaches, the construction of five hydropower stations, including Jinping I (2013), Jinping II (2013), Guandi (2012), Ertan (1999), and Tongzilin (2015), has significantly altered the terrestrial water storage (Wu and Shen, 2007). For this study, the Yalong River basin was divided into ten sub-basins based on the distribution of hydrological stations, as depicted in Figure 2. Station coordinates and basic hydrological and meteorological data of the respective sub-basins are given in Table S2.¶

Deleted: Figure

Deleted: Figure

Deleted: Figure

Formatted: Font: Italic

Formatted: Font: Italic

and the amplitude of ΔS varied significantly, including sharp transitions. There were even individual negative values of net R in TZL. Such phenomena are closely related to the influence of reservoirs (including hydropower dams) on the net runoff in nested catchment segments, where monthly outflow may be lower than monthly inflow, for instance when a hydropower dam near the outlet of a nested catchment temporarily stores more water (ΔS_{dam}) than what is created from local (positive) $R+\Delta S$ just upstream of the dam.

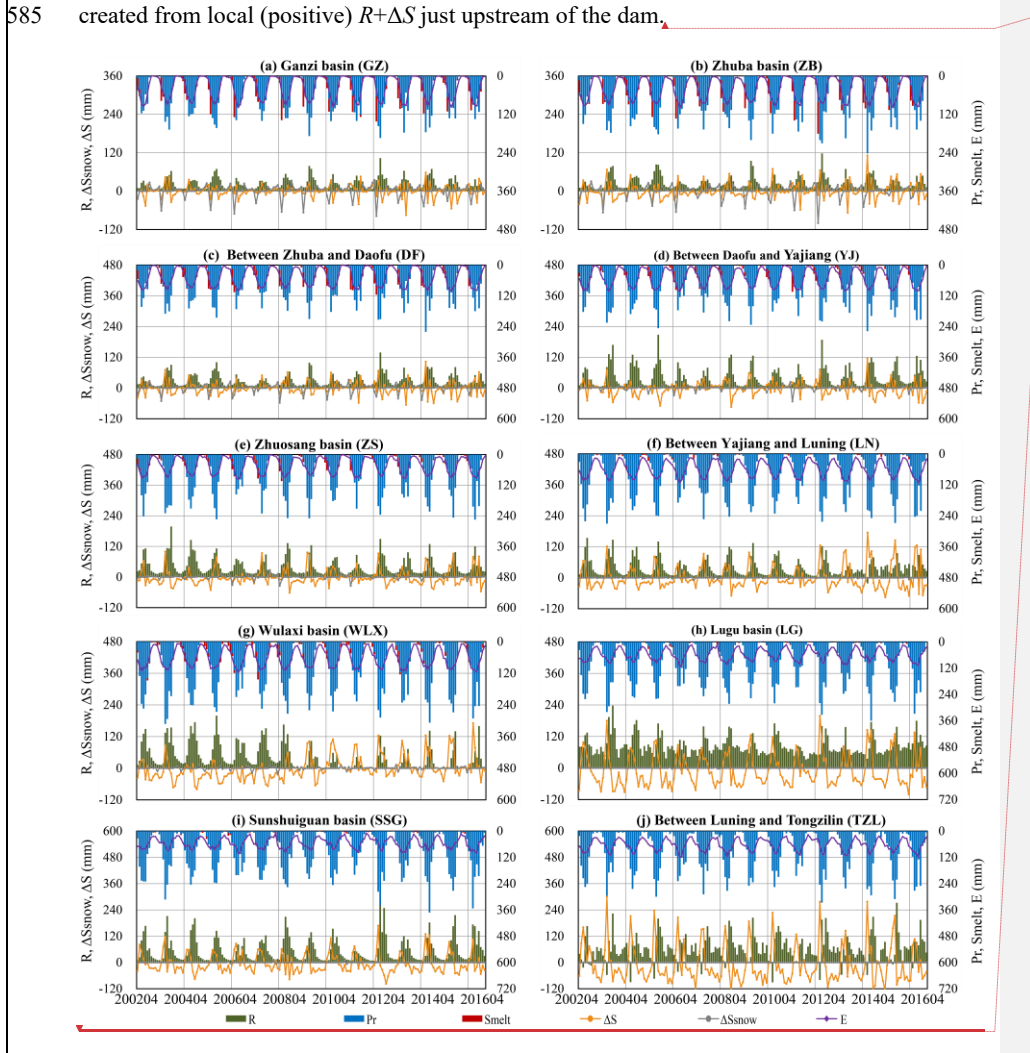
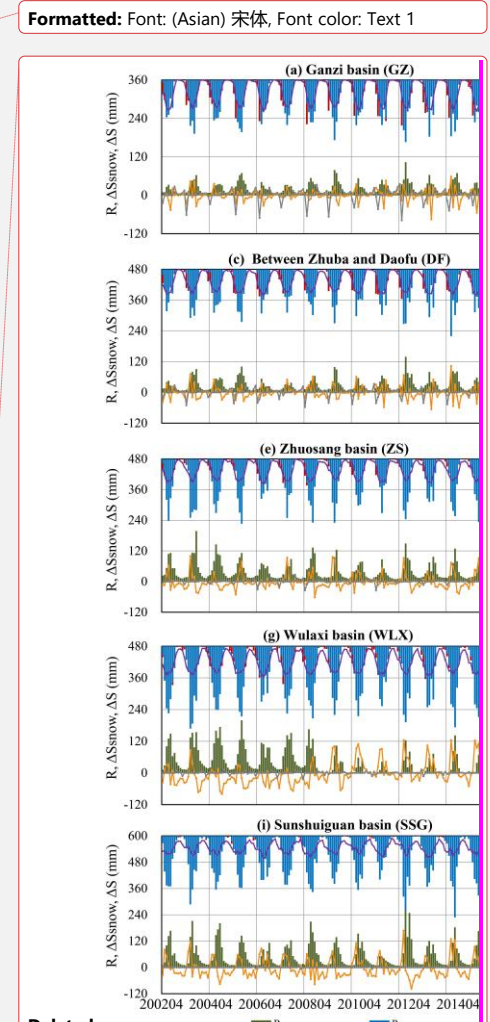


Figure 3. Time series of runoff (R), rainfall (P_r), snowmelt (S_{melt}), total storage change (ΔS), snow storage



Deleted:

change (ΔS_{snow}) and evapotranspiration (E) from 2002 to 2016 in the 10 sub-basins.

590

595

600

605

To further examine the intra-annual characteristics of key hydrological variables, Fig. 4 illustrates the average monthly time series of P, P_r , S_{melt} , ΔS , E, and R across the 10 sub-basins from 2002 to 2016. Differences between P and P_r are due to Ps and occurred primarily in the middle and upper regions including GZ and ZB during October to April. The Smelt, which is mainly caused by rising spring temperatures, reflects a delayed impact of P_s on runoff. Peak values of Smelt occurred between March and May. Constrained by the potential evapotranspiration and water supply conditions, E steadily increased from January to July, reaching its peak value in July before declining until December. R was positively correlated to P_r as as shown in Section 3.2, while ΔS primarily was positive during spring and summer, reflecting water storage. The contrasting negative ΔS during autumn and winter reflects water release. The maximum positive value of ΔS was typically observed in June because of the P_r and Smelt characteristics. The intra-annual variability of ΔS was more pronounced in the downstream basin compared to the upstream, which emphasizes the increasing impacts of flow regulation. The net R in the nested TZL-catchment exhibited a minimum (negative) value in June, coinciding with a maximum value of ΔS . This reflects a situation where the local water storage consists of considerable water volumes created upstream of the nested catchment itself. Such storage ensured high *R* in LG and TZL during the dry season.

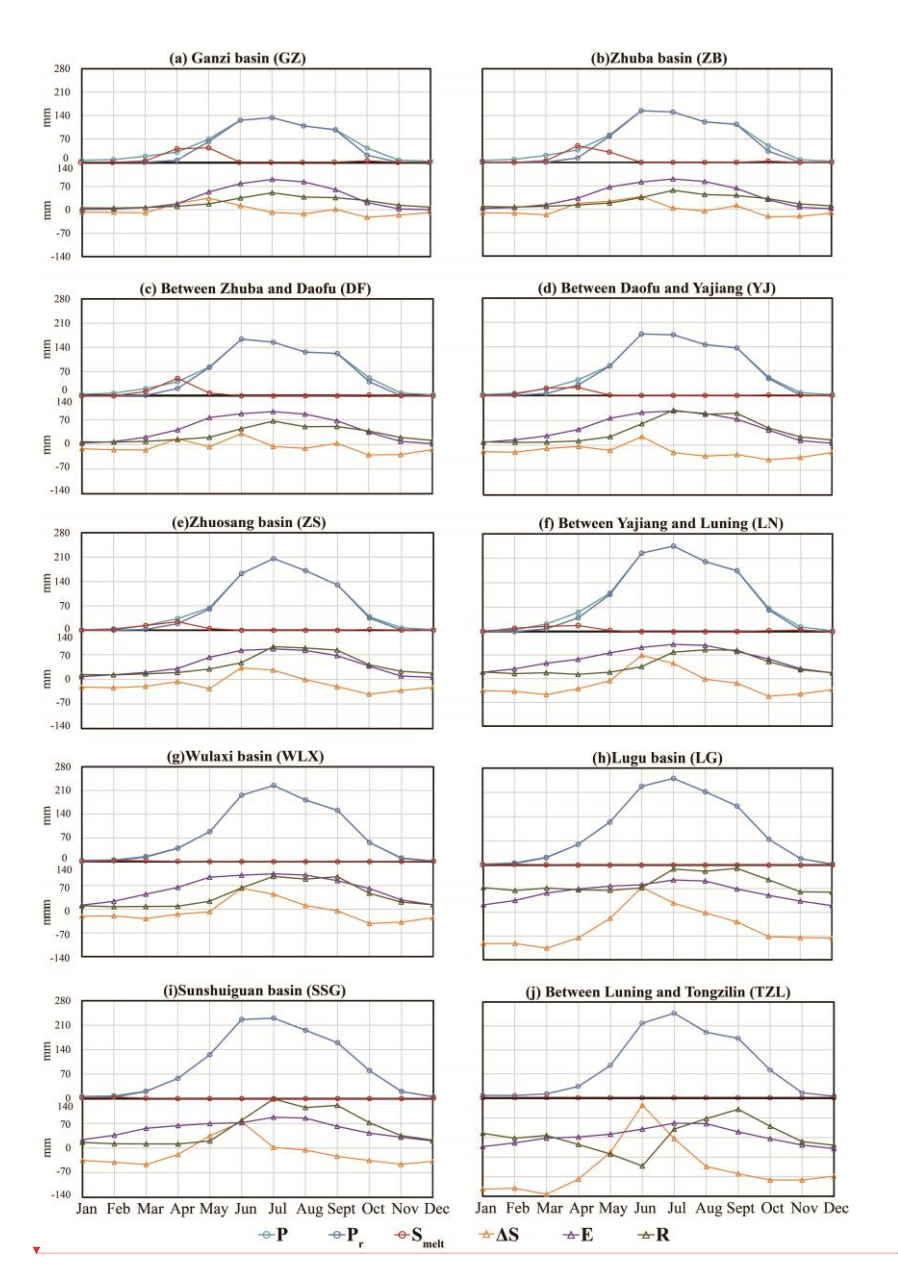


Figure 4. Annual average monthly P, P_r , S_{melt} , ΔS , E, and R from 2002 to 2016.

The relative contribution of the different water balance terms varies across seasons and

regions (Fig S1). P_r was generally the main contributor across catchments during May-October,

Deleted: ¶

while in most catchments $\Delta S'$ was the main contributor during January-April and November-December. It is noteworthy to mention that the proportions of P_r and S_{melt} in the high elevation catchments of GZ (in January, February, November, and December), ZB (in January, February, and December), DF (in January and December), and YJ (in December) were all 0%, as snow accumulation due to temperatures below 0°C essentially prevented effective water input into these basins. During this period, $\Delta S'$ were primarily driven by the output terms of R and E, although their values were low (Fig. 4).

3.2. Monthly runoff response to different factors

615

620

625

630

635

Partial correlation analysis was conducted after detrending to examine relationships between monthly R and each of its driving factors P_r , S_{melt} , ΔS , and E. As shown in Fig. 5, the results revealed strong positive correlations between R and P_r , however mainly around the summer period (May-Sept) only. There were considerable differences between the catchments, with the highest correlation coefficient observed for the low-elevation small headwater catchment of SSG between March and September (reaching 0.87 in May) and the overall lowest correlations found in the large central and nested catchment of LN where statistical significance was only obtained for May. Conversely, robust negative correlations between R and ΔS were observed from September to January. The correlations were remarkably strong throughout almost all subcatchments. They were e.g. significant in 8 out of 10 catchments in November, 10 out of 10 in December (including a peak correlation of -0.98 in TZL), and 9 out of 10 in January. The effect reflects an increased dominance of ΔS as a source of R, which is in wintertime can be explained by negligible P_r , S_{melt} and E. Furthermore, in the downstream catchments including LG and TZL, ΔS continues to be a dominating source of R throughout the year, reflecting that ΔS most likely boosted by reservoir storage to values well above those of Pr, Smelt and E. This is hence in contrast to upstream catchments including GZ, ZB, DF, YJ,

Deleted: downtrending

Deleted: Figure

Deleted: ¶

Moved (insertion) [3]

645

650

and ZS, which with few exceptions do not exhibit significant correlations between R and ΔS between March and August. From January to May, S_{melt} served as an additional contributor to locally created R during one or more months in all sub-basins except for the downstram-most TZL (Fig. 5). Regarding correlations between R and E they were found to be positive particularly in spring and early summer, probably because an increased availability of effective water supports simultaneous increases in R and E. In August however, correlations were negative in all of the investigated basins (Fig. 5) implying pronounced losses to the atmosphere.

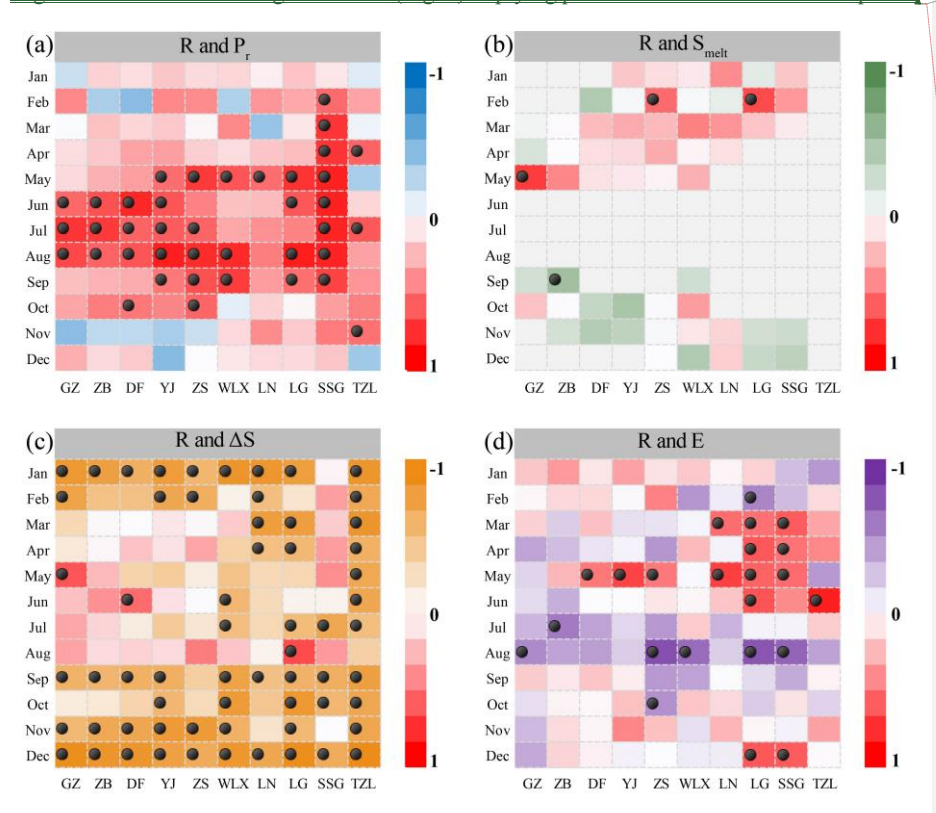


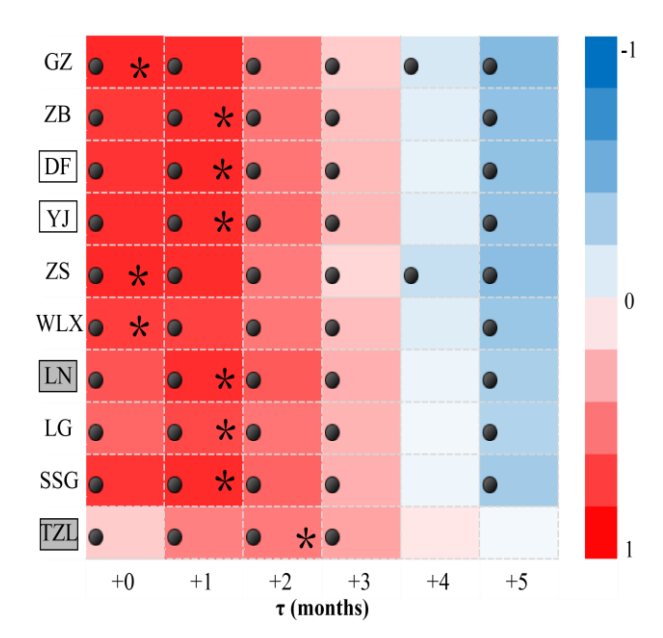
Figure 5. Correlation matrices between monthly R and its driving factors $(P_r, S_{melt}, \Delta S, \text{ and } E)$ during the 2002-2016 period in all sub-basins (GZ to TZL). The colors indicate the degree of correlation with darker colors reflecting stronger correlations. The dots represent significant correlations (p \leq 0.05).

The delayed effect of P on R was investigated considering the entire study period from

Moved up [3]: Conversely, robust negative correlations between R and ΔS were observed from September to January. The correlations were remarkably strong throughout almost all subcatchments. They were e.g. significant in 8 out of 10 catchments in November, 10 out of 10 in December (including a peak correlation of -0.98 in TZL), and 9 out of 10 in January. The effect reflects an increased dominance of ΔS as a source of R, which is in wintertime can be explained by negligible P_r , S_{melt} and E. Furthermore, in the downstream catchments including LG and TZL, ΔS continues to be a dominating source of R throughout the year, reflecting that ΔS most likely boosted by reservoir storage to values well above those of P_r , S_{melt} and E. This is hence in contrast to upstream catchments including GZ, ZB, DF, YJ, and ZS, which with few exceptions do not exhibit significant correlations between R and ΔS between March and August. From January to May, Smelt served as an additional contributor to locally created R during one or more months in all subbasins except for the downstram-most TZL (Fig. 5). Regarding correlations between R and E they were found to be positive particularly in spring and early summer, probably because an increased availability of effective water supports simultaneous increases in R and E. In August however, correlations were negative in all of the investigated basins (Fig. 5) implying pronounced losses to the atmosphere.

Deleted:

2002 to 2016 (Fig. 6). When $\tau = 0$, indicating R responses to P in the same month, the upper and middle reaches of the basin exhibited higher correlations, with the headwater catchments of GZ (0.85), ZS (0.84), and WLX (0.74) showing significant correlations. Conversely, LN (0.67), LG (0.60), and TZL (0.2) had relatively lower correlation coefficient values. A delay of $\tau = 1$ resulted in better P-R correlations for many basins, including all of the nested (non-headwater) basins DF (0.84), YJ (0.83), LN (0.82), and TZL (0.5) of which the latter two additionally contain hydropower dams. However, as the lag time increased to 2 and 3 months, correlations significantly started to weaken, except for the downstream-most TZL, which showed the most significant correlation (0.61) at a lag of two months. These results demonstrate that upstream mountainous headwater catchments on average exhibited relatively prompt R responses to P, despite seasonal snow storage, whereas ($\tau \ge 1$) in downstream nested catchments including those containing hydropower dams that may have effectively altered the natural precipitation-runoff response.



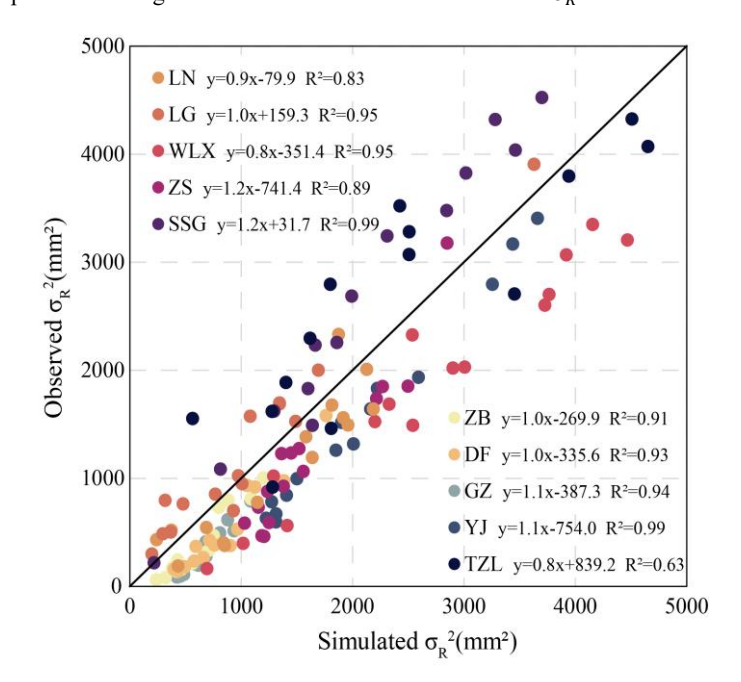
700

705

Figure 6. Correlation matrix between R and P during the period 2002-2016 in all sub-basins (GZ to TZL; nested sub-basins have rectancles around their names, with additional grey shading if they contain hydropower dams). The lagged response in months between R and P is denoted " τ ". The colors indicate the degree of correlation with darker colors reflecting stronger correlations. The dots represent significant correlations (p \leq 0.05). Each basin's best fitted τ is indicated by an asterisk.

3.3. Contribution of different factors to runoff variability

Using the Budyko-based variance decomposition method, the influence of various factors on the intra-annual variance of runoff (σ_R^2) in the ten sub-basins during the period 2002 to 2016 was quantified, as illustrated in Fig. 7. The determination coefficients R^2 of all sub-basins were greater than or equal to 0.9, except for LN (0.83), ZS (0.89), and TZL (0.63). The slope of the LG, ZB, and DF were 1.0, while SSG and YJ reached a maximum R^2 of 0.99. Substantially, the variance and covariance of P_r , S_{melt} , E_0 , and $\Delta S'$ effectively captured σ_R^2 , which emphasized the significant contribution of these factors to σ_R^2 .



Deleted: τ

Deleted: Figure

Figure 7. Relationships between the observed σ_R^2 and the simulated σ_R^2 (Eq. 15) using Budyko-based framework in all sub-basins.

715

720

725

of 5 to -20%.

Fig. 8 illustrates the relative contribution matrix of how variances and covariances of

water balance terms contribute to the runoff variance σ_R^2 . On average, $\sigma_{P_r}^2$ was the primary factor driving the intra-annual variance of runoff σ_R^2 in the 10 sub-basins, contributing more than 40%, except for TZL (30.2%) and LG (36.6%). The contribution of $\sigma_{\Delta S'}^2$ to σ_R^2 did not exceed 20%, except for TZL (24.3%). Among the covariance contribution of driving factors, $cov(P_r, \Delta S')$ had a significant impact on σ_R^2 , reaching a maximum value of 43.3% in LG. The contributions of other factors were limited, within 10%. These findings indicated that variation in P_r and $\Delta S'$ were the primary drivers of intra-annual R variability in the Yalong River basin, with the contribution of P_r variation being most prominent in the middle reaches. The impact of $\Delta S'$ variability was primarily observed downstream, while S_{melt} variability primarily affected the upstream reaches. The magnitude of contribution of the variances and covariances of the water balance terms to R variability is presented in Fig. S2. The impact of $\sigma_{E_0}^2$ and $cov(P_r, S_{melt})$, on σ_R^2 in the upper and middle reaches of the basin was highly volatile. The contribution of $cov(P_r, \Delta S')$ had a significant negative impact on σ_R^2 , reaching a maximum value of -48% in

LG, and the contributions of $cov(P_r, S_{melt})$, $cov(P_r, E_0)$, and $cov(S_{melt}, \Delta S')$, were all in the range

Deleted: Figure

Deleted: Figure

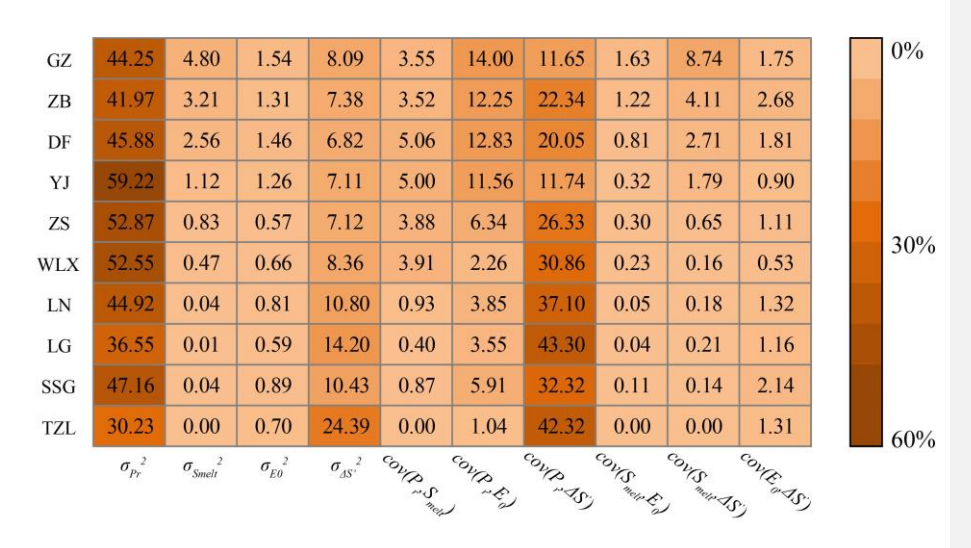


Figure 8. Relative contribution matrix of how variances in different water balance terms $(\sigma_{P_r}^2, \sigma_{S_{melt}}^2, \sigma_{E_0}^2)$, and $\sigma_{\Delta S'}^2$ and the covariances $cov(P_r, S_{melt}), cov(P_r, \Delta S'), cov(P_r, E_0), cov(S_{melt}, \Delta S'), cov(S_{melt}, E_0)$, and $cov(E_0, \Delta S')$ contribute to runoff variance (σ_R^2) during the period 2002-2016 in all sub-basins. The colors indicate the degree of contribution.

4. Discussion

735

740

745

4.1. Contributions of S_{melt} and ΔS to monthly runoff

This study considered the individual contributions of snow storage ΔS_{snow} and other storage components $\Delta S'$ (reservoirs, lakes, soil water, groundwater) on monthly runoff in the context of the Budyko framework (Bai et al., 2018; Hwang and Devineni, 2022; Shi and Gao, 2022). The findings suggest that ΔS_{snow} and the associated meltwater term S_{melt} played a prominent role as a source of runoff in the spring hydrological processes, which is consistent with other research findings e.g. by Huang et al. (2018). Present results supported previous results also regarding the dominance of $\Delta S'$ as a source of R in the downstream regions (Huang et al., 2021; Xu et al., 2012). This dominance in recent years has been reinforced by increased

storage in hydropower reservoirs within the Yalong River basin (e.g., Huang et al., 2021; Ning et al., 2024; Wu et al., 2024; Xu et al., 2012). However, in contrast to the decreased runoff seasonality that e.g. is found in snow-dominated rivers of central Europe (Rottler et al., 2020), the present study showed that the snow thinning (decreasing ΔS_{snow} ; Wu et al., 2024) seen in the upper snow dominated sub-catchments of the Yalong River basin is not yet clearly mirrored in runoff seasonality trends (Fig. 3). A contributing factor was found to be the relatively high runoff sensitivity to unfrozen precipitation (rain; Fig. 8). Nevertheless, results also showed that, in the upstream Yalong sub-catchments, the seasonal storage of snow still constitutes a large part of the total seasonal water storage (Fig. 3). As temperatures rise, the transition of precipitation from snow to rain in high-elevation regions may lead to earlier snowmelt, thus changing the timing and intensity of runoff. This implies that future runoff seasonality is at risk of decreasing if the climate-driven snow thinning of China's cold regions (Wu et al., 2024; Yang et al., 2015) will continue. Additionally, based on the applied nested catchment/ Budyko approach, this study contributed to disentangling some of the knowledge gaps related to the acknowledged (Fang et al., 2019) complex spatio-temporal runoff patterns in China's cold regions. In particular, we showed that the snow influence propagates to downstream snow-free regions; as e.g. seen in Fig. S3, snowmelt contributes approximately 6% to the annual runoff at the Yalong River outlet (Qi et al., 2022). Furthermore, the construction of large reservoirs in 1999 and 2013, mainly in the downstream part of the Yalong River basin, has redistributed the intra-annual runoff pattern of the lower basin (Fig. S3, Liu et al., 2019). We here showed that reservoirs contribute approximately 7% to the annual runoff at the Yalong River outlet (Fig. S3), primarily during January to April. Hence, snow storage and reservoir storage is currently of about the same importance for monthly runoff characteristics of the entire Yalong River basin, with the relative impact of snow processes and Smelt being considerably larger in its upstream parts. Additionally, since changed snow storage did not yet decrease runoff variability

750

755

760

765

in the snow-covered upstream part of the basin, it cannot have contributed to the recent-year decreases total runoff variability of the entire basin either (Fig. S3, top panel).

Regarding water availability present results showed that, for most of the year, there was sufficient water for P_r to simultaneously replenish both R and ΔS , resulting in a positive correlation between P_r and R (Fig. 5a). During the relatively cold dry season, R was then supplemented by consuming ΔS (negative correlation in Fig. 5c), thus highlighting the crucial role of ΔS in ensuring the availability of water resources throughout the year (Fig. 4). However, with rising temperatures, P_{L} and S_{melt} will increasingly be partitioned into E and decreasingly into R and/or ΔS during prolonged non-frozen (Condon et al., 2020; Zhang et al., 2015). This disturbs the balance of water supply and demand (Zhang et al., 2016) and calls for further research on the availability of ΔS to regulate and sufficiently redistribute R among rainy and dry seasons is essential considering the multiple and partially contrasting needs from energy demand, food demand and other human consumption.

4.2. Uncertainties and model performance evaluations

780

785

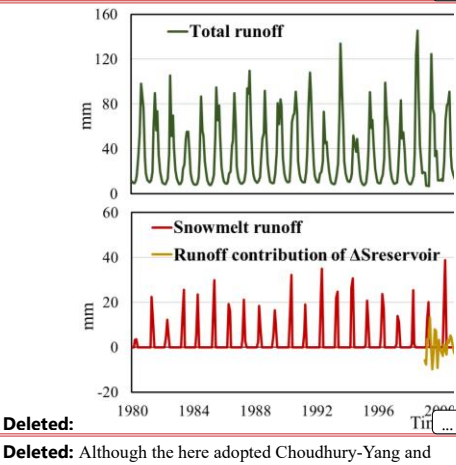
790

Although the Choudhury-Yang and Penman-Monteith equations adopted here are widely used for estimating actual and potential evapotranspiration, their site-specific applications involve uncertainties related to both parameters and processes, for instance, the under-studied evaporation mechanism under snow cover conditions (Gan et al., 2022). Since potential errors in E-estimations may translate into our $\Delta S'$ -results when we close water balances, we here independently check the E-estimation consistency by comparing the simulated E from the extended Budyko framework with remote sensing-derived E (GLEAM). The comparison showed good agreement (Table <u>\$2</u>), with Nash-Sutcliffe Efficiency (NSE) coefficients exceeding 0.8 for all 10 sub-basins, indicating high model accuracy and reliability. Furthermore, regarding seasonal water supply and demand, the relationship between the monthly ratio of

Moved (insertion) [1]

Moved up [1]: Regarding water availability present results showed that, for most of the year, there was sufficient water for P_r to simultaneously replenish both R and ΔS , resulting in a positive correlation between P_r and R (Fig. 5a). During the relatively cold dry season, R was then supplemented by consuming ΔS (negative correlation in Fig. 5c), thus highlighting the crucial role of ΔS in ensuring the availability of water resources throughout the year (Fig. 4). However, with rising temperatures, P_r and S_{melt} will increasingly be partitioned into E and decreasingly into R and/or ΔS during prolonged non-frozen (Condon et al., 2020; Zhang et al., 015). This disturbs the balance of water supply and demand (Zhang et al., 2016) and calls for further research on the availability of ΔS to regulate and sufficiently redistribute R among rainy and dry seasons is essential considering the multiple and partially contrasting needs from energy demand, food demand and other human consumption.

Deleted: This study considered the individual contributions of snow storage ΔS_{snow} and other storage components ΔS (reservoirs, lakes, soil water, groundwater) on monthly runoff in the context of the Budyko framework (Bai et al., 2018 Hwang and Devineni, 2022; Shi and Gao, 2022). The findings suggest that ΔS_{snow} and the associated meltwater term S_{melt} played a prominent role as a source of runoff in the spring hydrological processes, which is consistent with other research findings e.g. by Huang et al. (2018). Present results supported previous results also regarding the dominance of $\Delta S'$ as a source of R in the downstream regions (Huang et al., 2021; Xu et al., 2012). This dominance has in recent years has been reinforced by increased storage in hydropower reservoirs within the Yalong River basin (e.g., Huang et al., 2021; Ning et al., 2024; Wu et al., 2024; Xu et al., 2012). However, in contrast to the decreased runoff seasonality that e.g. is found in snow-dominated rivers of central Europe (Rottler et al., 2020), the present study showed that the sno



Deleted: Although the here adopted Choudhury-Yang and Penman-Monteith equations

Deleted: are associated with

Deleted: such as

Deleted: S3

water demand to water supply $(E/(P_r + S_{melt} - \Delta S'))$ and monthly ratio of potential water demand to water supply $(E_0/(P_r + S_{melt} - \Delta S'))$ as expressed in the extended Budyko framework was further examined for three representative basins: LN, YJ and ZS (Fig. <u>S4</u>). Water supply constraints typically occurred in the spring, while water demand constraints were more prevalent in the summer and autumn.

905

910

915

920

925

Regarding the partitioning of P into corresponding P_r and P_s components including e.g. snow melt S_{melt} processes, we recognize that there are several challenges of determining temperature threshold values. These include impacts of solar radiation on snowmelt (Liu et al., 2017), as well as topography and hydrometeorological factors, particularly in mountainous regions, where topographical elements such as slope, aspect, and mountain cover exert a substantial influence on snow melting (Gan et al., 2022). The energy exchange of snow is furthermore a dynamic process that undergoes temporal variations, leading to discrepancies in the timescales of degree-day factors across different zones (Zhang et al., 2006). In this study, a dataset with the spatial distribution of degree-day factors for glaciers in High Mountain Asia was employed, for which its accuracy had been verified through typical regional simulation applications (Zhang et al., 2016; Zhang et al., 2017). The fact that the degree-day factor method yielded satisfactory simulation results at both daily and monthly time scales (Zhang et al., 2016; 2017) underpins the assumption that our can effectively utilized to calculate monthly snow melt in the here considered Yalong River basin (see also Wu et al., 2024). At the same time, we acknowledge that remaining, difficult-to-reduce process and parameter uncertainties may have

Facing such remaining uncertainties, we independently ascertained that our main (model-derived) results were consistent with actual, site-specific water storage change outcomes. This was done by collecting and taking advantage of daily storage and release data from several reservoirs within the downstream, nested TZL sub-basin (in which ΔS_{snow} =0). This sub-basin

non-negligible impacts the presented results.

Deleted: S3

Moved (insertion) [2]

includes the Ertan, Tongzilin and Guandi hydropower reservoirs, which due to their considerable size together represent a large part of the sub-basin's water storage change ΔS , making it reasonable to assume that $\Delta S_{Reservoirs} \approx \Delta S$. This hence provides a means to constrain and verify our estimates regarding the magnitudes and characteristics of ΔS dynamics, which were derived through water balance closure. We therefore assessed the agreement between the combined monthly storage changes of these reservoirs $\Delta S_{Reservoirs}$ and our estimated storage change ΔS , as illustrated in Fig. S5. The figure specifically shows that the estimated dynamics of ΔS fully encloses the amplitudes and reproduces the trends of observed $\Delta S_{Reservoirs}$. Regarding the differences in magnitude of storage change, the standard deviation of estimated ΔS was 86mm, which can be compared with the standard deviation of observed ΔS_{Reservoirs} of 46mm. This hence suggests that reservoirs account for about 53% of the estimated total water storage changes, with the missing part originating from unmonitored contributions e.g. stemming from storage changes in groundwater reservoirs, unmonitored surface water reservoirs and soil water. From a methodological viewpoint, we note that the value of 53% also provides an upper limit on our possible overestimation of ΔS , for the unlikely case that storage changes in groundwater reservoirs, unmonitored surface water reservoirs and soil water of TZL would in fact be negligible (i.e. approximately equal to 0), such that the differences in storage changes between the two curves of Fig. S5 would be entirely due to errors in snow melt modelling and water balance closure. However, even for such lowest possible limit value of actual ΔS , the storage volumes are still considerable. These findings hence highlight the critical role that reservoirs, influenced by human activities, can increasingly play in modulating surface water storage in high-mountain areas subject to climate change.

5. Conclusions

930

935

940

945

950

Deleted: ¶

This study employed an extended Budyko framework in 10 nested catchments of the cold

and mountainous Yalong River basin, to analyze spatio-temporal characteristics in water balance terms, and to identify main drivers of monthly runoff variability across an elevation gradient (from 5,900 to 1,000 m.a.s.l.). The main findings of this study are:

960

965

970

975

980

- 1) Snow accumulation and snowmelt are main drivers of runoff seasonality in the upper sub-catchments of the Yalong River basin, with propagating impacts also on lower elevation snow-free sub-catchments. These are under increasing additional influence of hydropower reservoirs, creating a relatively strong altitudinal heterogeneity in drivers of monthly runoff. Similar elevation-dependent mechanisms may occur in other snow-affected basins, such as Alpine-origin rivers in Europe, though further high-resolution studies are needed to confirm this.
- 2) Presently, snow storage and reservoir storage have approximately equal contributions (6-7% each) to discharge at the Yalong River outlet at its confluence with the Yangtze River, implying that both factors need to be accounted for in predictive models.
- 3) Snow thinning in the high-elevation, snow dominated sub-catchments of the Yalong River basin is not yet clearly mirrored in time-series of high-elevation runoff seasonality, e.g. due to a considerable runoff sensitivity to unfrozen precipitation.
- 4) The observed lowered runoff seasonality in the lower Yalong River basin (at its Yangtze River outlet) is therefore not snow-related and hence likely caused by trends in unfrozen precipitation seasonality and/or flow-modulating impacts of constructed reservoirs, natural lakes and groundwater, implying that continued snow thinning may further exacerbate such trends in the future.
- 5) Regarding lag times, the upstream mountainous headwater catchments of the Yalong basin showed relatively prompt runoff (R) responses to precipitation (P), with lag times (z) of one month or less (i.e., $\tau \le 1$), despite the presence of seasonal snow storage. In contrast,

Deleted: This is hypothesized to occur also in other world regions including e.g. major European rivers of Alpine origin, although not yet quantified at similarly high spatio-temporal resolution as in the current study.

Deleted: Presently, snow storage and reservoir storage have approximately equal contributions (6-7% each) to discharge at the Yalong River outlet at its confluence with the Yangtze River, implying that both factors need to be accounted for in predictive models.¶

Deleted: <#>Snow thinning in the high-elevation, snow dominated sub-catchments of the Yalong River basin is not yet clearly mirrored in time-series of high-elevation runoff seasonality, e.g. due to a considerable runoff sensitivity to unfrozen precipitation.

The observed lowered runoff seasonality in the lower Yalong River basin (at its Yangtze River outlet) is therefore not snow related and hence likely caused by trends in unfrozen precipitation seasonality and/or flow-modulating impacts of constructed reservoirs, natural lakes and groundwater, implying that continued snow thinning may further exacerbate such trends in the future.

Formatted: Font: Italic

Formatted: Font: Italic

Formatted: Font: Italic

Formatted: Font: Italic

1005

downstream nested catchments, including those containing man-made reservoirs, exhibited more significant delays (i.e., $\tau > 1$).

1010

1015

6) Methodologically, we showed by independent verification with reservoir storage data that the extended monthly Budyko framework could be used to distinguish between water storage and seasonal snow accumulation, which has important implications for understanding dominant runoff processes, and more generally for mitigating adverse effect related to the rapid environmental changes that the Yalong River basin and other cold regions (not least of the Tibetan plateau) are currently experiencing.

Author Contributions

N.W. and J.J. conceived the idea and designed the research framework. Z.N. carried out data collection, preprocessing, and method determination. N.W. and H.H. performed data analysis, graphical visualization, and manuscript preparation. K.Z. and A.N. contributed to manuscript refinement. All authors have read and agreed to the published version of the manuscript.

Acknowledgments

1020

This study was supported by the Fundamental Research Funds for the Central Universities of China: B240203007 and Fund of National Key Laboratory of Water Disaster Prevention: 524015222.

Declaration of competing interest

The authors declare that they have no known competing financial interests or personal relationships that could have appeared to influence the work reported in this paper.

Formatted: Font: Italic

Deleted: R responses to P (less than a month on average) despite seasonal snow storage, whereas delays were more significant (i.e., more than a month) in downstream nested catchments including those containing man-made reservoirs.

References

1030

•								
	Allen, R.G., Pereira, L.S., Raes, D., Smith, M., 1998. Crop evapotranspiration-Guidelines for							
	computing crop water requirements-FAO Irrigation and drainage paper 56. Food an							
	Agriculture Organization of the United Nations, Rome.							
	Bai, J., Li, J., Shi, H., Liu, T., Zhong, R., 2018. Snowmelt Water Alters the Regime of Runoff							
1035	in the Arid Region of Northwest China. Water 10, 902.							
	https://doi.org/10.3390/w10070902							
	Bao, Z., Zhang, Jianyun, Lian, Y., Wang, G., Jin, J., Ning, Z., Zhang, Jiapeng, Liu, Y., Wang,							
•	X., 2023. Changes in Headwater Streamflow from Impacts of Climate Change in the							
	Tibetan Plateau. Engineering. https://doi.org/10.1016/j.eng.2023.05.025							
1040	Berghuijs, W.R., Sivapalan, M., Woods, R.A., Savenije, H.H.G., 2014. Patterns of similarity of							
Į	seasonal water balances: A window into streamflow variability over a range of time scales.							
	Water Resour. Res. 50, 5638-5661. https://doi.org/10.1002/2014WR015692							
	Bounoua, L., DeFries, R.S., Imhoff, M.L., Steininger, M.K., 2004. Land use and local climate:							
•	A case study near Santa Cruz, Bolivia. Meteorol. Atmos. Phys. 86, 73-85.							
1045	https://doi.org/10.1007/s00703-003-0616-8							
	Brutsaert, W., Hiyama, T., 2012. The determination of permafrost thawing trends from long-							
•	term streamflow measurements with an application in eastern Siberia. J. Geophys. Res							
	Atmos. 117, D22110. https://doi.org/10.1029/2012JD018344							
	Chao, B.F., Wu, Y.H., Li, Y.S., 2008. Impact of Artificial Reservoir Water Impoundment on							
1050	Global Sea Level. Science 320, 212–214. https://doi.org/10.1126/science.1154580							
	Chen, D.L., Gao, G., Xu, C.Y., Guo, J., Ren, G.Y., 2005. Comparison of the Thornthwaite							
•	method and pan data with the standard Penman-Monteith estimates of reference							
	evapotranspiration in China. Clim. Res. 28, 123-132. https://doi.org/10.3354/cr028123							
	Choudhury, B.J., 1999. Evaluation of an empirical equation for annual evaporation using field							
1055	observations and results from a biophysical model. J. Hydrol. 216, 99-110.							
	https://doi.org/10.1016/S0022-1694(98)00293-5							
	Condon, L.E., Atchley, A.L., Maxwell, R.M., 2020. Evapotranspiration depletes groundwater							
·	under warming over the contiguous United States. Nat. Commun. 11, 873.							
	https://doi.org/10.1038/s41467-020-14688-0							
1060	Cui, T., Li, Y., Yang, L., Nan, Y., Li, K., Tudaji, M., Hu, H., Long, D., Shahid, M., Mubeen, A.,							
•	He, Z., Yong, B., Lu, H., Li, C., Ni, G., Hu, C., Tian, F., 2023. Non-monotonic changes in							
	34							

Formatted: Indent: Left: 0 cm, Hanging: 2 ch, First line: -2 ch, Line spacing: 1.5 lines

- Asian Water Towers' streamflow at increasing warming levels. Nat. Commun. 14, 1176. https://doi.org/10.1038/s41467-023-36804-6
- Dethier, E.N., Sartain, S.L., Renshaw, C.E., Magilligan, F.J., 2020. Spatially coherent regional changes in seasonal extreme streamflow events in the United States and Canada since 1950. Sci. Adv. 6, eaba5939. https://doi.org/10.1126/sciadv.aba5939
 - Du, C., Sun, F., Yu, J., Liu, X., Chen, Y., 2016. New interpretation of the role of water balance in an extended Budyko hypothesis in arid regions. Hydrol. Earth Syst. Sci. 20, 393–409. https://doi.org/10.5194/hess-20-393-2016
- 1070 Fang, H., Huang, L., Wang, J., He, G., Reible, D., 2016. Environmental assessment of heavy metal transport and transformation in the Hangzhou Bay, China. J. Hazard. Mater. 302, 447–457. https://doi.org/10.1016/j.jhazmat.2015.09.060

1075

1085

- Fang, Y., Li, H., Wan, W., Zhu, S., Wang, Z., Hong, Y., Wang, H., 2019. Assessment of Water Storage Change in China's Lakes and Reservoirs over the Last Three Decades. Remote Sens. 11, 1467. https://doi.org/10.3390/rs11121467
- Gan, G., Wu, J., Hori, M., Fan, X., Liu, Y., 2022. Attribution of decadal runoff changes by considering remotely sensed snow/ice melt and actual evapotranspiration in two contrasting watersheds in the Tienshan Mountains. J. Hydrol. 610, 127810. https://doi.org/10.1016/j.jhydrol.2022.127810
- 1080 Gao, H., Ding, Y., Zhao, Q., Hrachowitz, M., Savenije, H.H.G., 2017. The importance of aspect for modelling the hydrological response in a glacier catchment in Central Asia. Hydrol. Process. 31, 2842–2859. https://doi.org/10.1002/hyp.11224
 - Guo, W., Teng, Y., Li, J., Yan, Y., Zhao, C., Li, Y., Li, X., 2024. A new assessment framework to forecast land use and carbon storage under different SSP-RCP scenarios in China. Science of The Total Environment 912, 169088. https://doi.org/10.1016/j.scitotenv.2023.169088
 - Gutenson, J.L., Tavakoly, A.A., Wahl, M.D., Follum, M.L., 2020. Comparison of generalized non-data-driven lake and reservoir routing models for global-scale hydrologic forecasting of reservoir outflow at diurnal time steps. Hydrol. Earth Syst. Sci. 24, 2711–2729. https://doi.org/10.5194/hess-24-2711-2020
 - Han, P., Long, D., Han, Z., Du, M., Dai, L., Hao, X., 2019. Improved understanding of snowmelt runoff from the headwaters of China's Yangtze River using remotely sensed snow products and hydrological modeling. Remote Sens. Environ. 224, 44–59. https://doi.org/10.1016/j.rse.2019.01.041

1095 He, Z., Zhang, X., Bao, S., Qiao, Y., Sheng, Y., Liu, X., He, X., Yang, X., Zhao, J., Liu, R., Lu, C., 2015. Multiple climatic cycles imprinted on regional uplift-controlled fluvial terraces in the lower Yalong River and Anning River, SE Tibetan Plateau. Geomorphology 250, 95–112. https://doi.org/10.1016/j.geomorph.2015.08.010

1100

1110

1115

1125

- Hock, R., 2003. Temperature index melt modelling in mountain areas. J. Hydrol. 282, 104–115. https://doi.org/10.1016/S0022-1694(03)00257-9
- Huang, P., Song, J., Cheng, D., Sun, H., Kong, F., Jing, K., Wu, Q., 2021. Understanding the intra-annual variability of streamflow by incorporating terrestrial water storage from GRACE into the Budyko framework in the Qinba Mountains. J. Hydrol. 603, 126988. https://doi.org/10.1016/j.jhydrol.2021.126988
- Huang, Y., Zhao, H., Jiang, Y., Lu, X., 2018. Runoff and its influencing factors in the upper reaches of the Yalong River. Arid Land Geo. 41, 127–133. https://doi.org/10.13826/j.cnki.cn65-1103/x.2018.01.016
 - Huo, J., Liu, C., Yu, X., Jia, G., Chen, L., 2021. Effects of watershed char and climate variables on annual runoff in different climatic zones in China. Sci. Total Environ. 754, 142157. https://doi.org/10.1016/j.scitotenv.2020.142157
 - Hwang, J., Devineni, N., 2022. An Improved Zhang's Dynamic Water Balance Model Using Budyko-Based Snow Representation for Better Streamflow Predictions. Water Resour. Res. 58, e2021WR030203. https://doi.org/10.1029/2021WR030203
 - Kazemi, H., Hashemi, H., Maghsood, F.F., Hosseini, S.H., Sarukkalige, R., Jamali, S., Berndtsson, R., 2021. Climate vs. Human Impact: Quantitative and Qualitative Assessment of Streamflow Variation. Water 13, 2404. https://doi.org/10.3390/w13172404
 - Kuhn, M., Helfricht, K., Ortner, M., Landmann, J., Gurgiser, W., 2016. Liquid water storage in snow and ice in 86 Eastern Alpine basins and its changes from 1970-97 to 1998-2006. Ann. Glaciol. 57, 11–18. https://doi.org/10.1017/aog.2016.24
- Li, L., Ni, J., Chang, F., Yue, Y., Frolova, N., Magritsky, D., Borthwick, A.G.L., Ciais, P., Wang, Y., Zheng, C., Walling, D.E., 2020. Global trends in water and sediment fluxes of the world's large rivers. Sci. Bull. 65, 62–69. https://doi.org/10.1016/j.scib.2019.09.012

https://doi.org/10.1016/j.scitotenv.2020.144244

- Li, X., Zhang, K., Gu, P., Feng, H., Yin, Y., Chen, W., Cheng, B., 2021. Changes in precipitation extremes in the Yangtze River Basin during 1960-2019 and the association with global warming, ENSO, and local effects. Sci. Total Environ. 760, 144244.
- Li, Z., Quiring, S.M., 2021. Investigating spatial heterogeneity of the controls of surface water

- balance in the contiguous United States by considering anthropogenic factors. J. Hydrol. 601, 126621. https://doi.org/10.1016/j.jhydrol.2021.126621
- Liu, J., You, Y., Zhang, Q., Gu, X., 2021. Attribution of streamflow changes across the globe based on the Budyko framework. Sci. Total Environ. 794, 148662. https://doi.org/10.1016/j.scitotenv.2021.148662

1145

- Liu, J., Zhang, Q., Feng, S., Gu, X., Singh, V.P., Sun, P., 2019. Global Attribution of Runoff Variance Across Multiple Timescales. J. Geophys. Res.-Atmos. 124, 13962–13974. https://doi.org/10.1029/2019JD030539
- Liu, J., Zhang, Q., Singh, V.P., Shi, P., 2017. Contribution of multiple climatic variables and human activities to streamflow changes across China. J. Hydrol. 545, 145–162. https://doi.org/10.1016/j.jhydrol.2016.12.016
- Liu, J., Zhang, Q., Singh, V.P., Song, C., Zhang, Y., Sun, P., Gu, X., 2018. Hydrological effects of climate variability and vegetation dynamics on annual fluvial water balance in global large river basins. Hydrol. Earth Syst. Sci. 22, 4047–4060. https://doi.org/10.5194/hess-22-4047-2018
 - Liu, X., Yang, M., Meng, X., Wen, F., Sun, G., 2019. Assessing the Impact of Reservoir Parameters on Runoff in the Yalong River Basin using the SWAT Model. Water 11, 643. https://doi.org/10.3390/w11040643
 - Liu, Z., Wang, T., Han, J., Yang, W., Yang, H., 2022. Decreases in Mean Annual Streamflow and Interannual Streamflow Variability Across Snow-Affected Catchments Under a Warming Climate. Geophys. Res. Lett. 49, e2021GL097442. https://doi.org/10.1029/2021GL097442
- l Luo, M., Lau, N.-C., 2018. Synoptic characteristics, atmospheric controls, and long-term changes of heat waves over the Indochina Peninsula. Clim. Dyn. 51, 2707–2723. https://doi.org/10.1007/s00382-017-4038-6
 - Lute, A.C., Abatzoglou, J.T., 2014. Role of extreme snowfall events in interannual variability of snowfall accumulation in the western United States. Water Resour. Res. 50, 2874–2888. https://doi.org/10.1002/2013WR014465
 - Miralles, D.G., De Jeu, R. a. M., Gash, J.H., Holmes, T.R.H., Dolman, A.J., 2011. Magnitude and variability of land evaporation and its components at the global scale. Hydrol. Earth Syst. Sci. 15, 967–981. https://doi.org/10.5194/hess-15-967-2011
- New, M., Hulme, M., Jones, P., 2000. Representing twentieth-century space-time climate variability. Part II: Development of 1901-96 monthly grids of terrestrial surface climate.

- J. Clim. 13, 2217–2238. https://doi.org/10.1175/1520-0442(2000)013<2217:RTCSTC>2.0.CO;2
- Ning, T., Li, Z., Liu, W., 2017. Vegetation dynamics and climate seasonality jointly control the interannual catchment water balance in the Loess Plateau under the Budyko framework. Hydrol. Earth Syst. Sci. 21, 1515–1526. https://doi.org/10.5194/hess-21-1515-2017

1175

1180

- Ning, Z., Wu, N., Zhang, J., Ruan, Y., Tang, Z., Sun, J., Shi, J., Liu, C., Wang, G., 2024. Wetter trend in source region of Yangtze River by runoff simulating based on Grid-RCCC-WBM. J. Hydrol. 631, 130702. https://doi.org/10.1016/j.jhydrol.2024.130702
- Qi, J., Wang, L., Zhou, J., Song, L., Li, X., Zeng, T., 2019. Coupled Snow and Frozen Ground
 Physics Improves Cold Region Hydrological Simulations: An Evaluation at the upper
 Yangtze River Basin (Tibetan Plateau). J. Geophys. Res.-Atmos. 124, 12985–13004.
 https://doi.org/10.1029/2019JD031622
 - Qi, W., Feng, L., Kuang, X., Zheng, C., Liu, J., Chen, D., Tian, Y., Yao, Y., 2022. Divergent and Changing Importance of Glaciers and Snow as Natural Water Reservoirs in the Eastern and Southern Tibetan Plateau. Journal of Geophysical Research: Atmospheres 127, e2021JD035888. https://doi.org/10.1029/2021JD035888
 - Rottler, E., Francke, T., Buerger, G., Bronstert, A., 2020. Long-term changes in central European river discharge for 1869-2016: impact of changing snow covers, reservoir constructions and an intensified hydrological cycle. Hydrol. Earth Syst. Sci. 24, 1721–1740. https://doi.org/10.5194/hess-24-1721-2020
 - Shen, C., 2018. A Transdisciplinary Review of Deep Learning Research and Its Relevance for Water Resources Scientists. Water Resour. Res. 54, 8558–8593. https://doi.org/10.1029/2018WR022643
 - Shi, G., Gao, B., 2022. Attribution Analysis of Runoff Change in the Upper Reaches of the Kaidu River Basin Based on a Modified Budyko Framework. Atmosphere 13, 1385. https://doi.org/10.3390/atmos13091385
 - Stigter, E.E., Litt, M., Steiner, J.F., Bonekamp, P.N.J., Shea, J.M., Bierkens, M.F.P., Immerzeel, W.W., 2018. The Importance of Snow Sublimation on a Himalayan Glacier. Front. Earth Sci. 6, 108. https://doi.org/10.3389/feart.2018.00108
- 1 Tu, X., Singh, V.P., Chen, X., Chen, L., Zhang, Q., Zhao, Y., 2015. Intra-annual Distribution of Streamflow and Individual Impacts of Climate Change and Human Activities in the Dongijang River Basin, China. Water Resour. Manag. 29, 2677–2695. https://doi.org/10.1007/s11269-015-0963-5

- Wang, D., Tang, Y., 2014. A one-parameter Budyko model for water balance captures emergent behavior in darwinian hydrologic models. Geophys. Res. Lett. 41, 4569–4577. https://doi.org/10.1002/2014GL060509
 - Wang, Z., Wu, R., Chen, S., Huang, G., Liu, G., Zhu, L., 2018. Influence of Western Tibetan Plateau Summer Snow Cover on East Asian Summer Rainfall. J. Geophys. Res.-Atmos. 123, 2371–2386. https://doi.org/10.1002/2017JD028016
- 1200 Widen-Nilsson, E., Halldin, S., Xu, C., 2007. Global water-balance modelling with WASMOD-M: Parameter estimation and regionalisation. J. Hydrol. 340, 105–118. https://doi.org/10.1016/j.jhydrol.2007.04.002

1215

- Wu, C., Yeh, P.J.-F., Hu, B.X., Huang, G., 2018. Controlling factors of errors in the predicted annual and monthly evaporation from the Budyko framework. Adv. Water Resour. 121, 432–445. https://doi.org/10.1016/j.advwatres.2018.09.013
- Wu, C., Yeh, P.J.-F., Wu, H., Hu, B.X., Huang, G., 2019. Global Analysis of the Role of Terrestrial Water Storage in the Evapotranspiration Estimated from the Budyko Framework at Annual to Monthly Time Scales. J. Hydrometeorol. 20, 2003–2021. https://doi.org/10.1175/JHM-D-19-0065.1
- 1210 Wu, N., Zhang, K., Chao, L., Ning, Z., Wang, S., Jarsjö, J., 2024. Snow cover expansion with contrasting depth thinning in the recent 40 years: Evidence from the Yalong River Basin, South-eastern Tibetan Plateau. J. Hydrol.-Reg. Stud. 53, 101786. https://doi.org/10.1016/j.ejrh.2024.101786
 - Wu S., Shen M., 2007. The key technical issue and its research advance in Yalong River hydropower development. J. Hydrau. Eng. 15–19.
 - Wu, Z., Li, J., Jiang, Z., Ma, T., 2012. Modulation of the Tibetan Plateau Snow Cover on the ENSO Teleconnections: From the East Asian Summer Monsoon Perspective. J. Clim. 25, 2481–2489. https://doi.org/10.1175/JCLI-D-11-00135.1
 - Wulf, H., Bookhagen, B., Scherler, D., 2016. Differentiating between rain, snow, and glacier contributions to river discharge in the western Himalaya using remote-sensing data and distributed hydrological modeling. Adv. Water Resour. 88, 152–169. https://doi.org/10.1016/j.advwatres.2015.12.004
- Xin, J., Sun, X., Liu, L., Li, H., Liu, X., Li, X., Cheng, L., Xu, Z., 2021. Quantifying the contribution of climate and underlying surface changes to alpine runoff alterations associated with glacier melting. Hydrol. Process. 35, e14069. https://doi.org/10.1002/hyp.14069

- Xin, Z., Li, Y., Zhang, L., Ding, W., Ye, L., Wu, J., Zhang, C., 2019. Quantifying the relative contribution of climate and human impacts on seasonal streamflow. J. Hydrol. 574, 936–945. https://doi.org/10.1016/j.jhydrol.2019.04.095
- 1230 Xu, X., Yang, D., Sivapalan, M., 2012. Assessing the impact of climate variability on catchment water balance and vegetation cover. Hydrol. Earth Syst. Sci. 16, 43–58. https://doi.org/10.5194/hess-16-43-2012

- Xu, X., Yang, D., Yang, H., Lei, H., 2014. Attribution analysis based on the Budyko hypothesis for detecting the dominant cause of runoff decline in Haihe basin. J. Hydrol. 510, 530–540. https://doi.org/10.1016/j.jhydrol.2013.12.052
- Yang, H., Yang, D., Lei, Z., Sun, F., 2008. New analytical derivation of the mean annual waterenergy balance equation. Water Resour. Res. 44, W03410. https://doi.org/10.1029/2007WR006135
- Yang, T., Wang, C., Chen, Y., Chen, X., Yu, Z., 2015. Climate change and water storage variability over an arid endorheic region. J. Hydrol. 529, 330–339. https://doi.org/10.1016/j.jhydrol.2015.07.051
 - Yang, Z., Bai, P., 2023. Evaporation from snow surface: A multi-model evaluation with the FLUXNET2015 dataset. J. Hydrol. 621, 129587. https://doi.org/10.1016/j.jhydrol.2023.129587
- 1245 Yao, L., Libera, D.A., Kheimi, M., Sankarasubramanian, A., Wang, D., 2020. The Roles of Climate Forcing and Its Variability on Streamflow at Daily, Monthly, Annual, and Long-Term Scales. Water Resour. Res. 56. https://doi.org/10.1029/2020WR027111
 - Ye, S., Li, H.-Y., Li, S., Leung, L.R., Demissie, Y., Ran, Q., Bloeschl, G., 2015. Vegetation regulation on streamflow intra-annual variability through adaption to climate variations. Geophys. Res. Lett. 42, 10307–10315. https://doi.org/10.1002/2015GL066396
 - Zeng, R., Cai, X., 2015. Assessing the temporal variance of evapotranspiration considering climate and catchment storage factors. Adv. Water Resour. 79, 51–60. https://doi.org/10.1016/j.advwatres.2015.02.008
- Zhang, D., Cong, Z., Ni, G., Yang, D., Hu, S., 2015. Effects of snow ratio on annual runoff within the Budyko framework. Hydrol. Earth Syst. Sci. 19, 1977–1992. https://doi.org/10.5194/hess-19-1977-2015
 - Zhang, D., Liu, X., Zhang, Q., Liang, K., Liu, C., 2016. Investigation of factors affecting intraannual variability of evapotranspiration and streamflow under different climate conditions. J. Hydrol. 543, 759–769. https://doi.org/10.1016/j.jhydrol.2016.10.047

1260 Zhang, K., Kimball, J.S., Nemani, R.R., Running, S.W., Hong, Y., Gourley, J.J., Yu, Z., 2015. Vegetation Greening and Climate Change Promote Multidecadal Rises of Global Land Evapotranspiration. Sci Rep 5, 15956. https://doi.org/10.1038/srep15956 Zhang, L., Hickel, K., Dawes, W.R., Chiew, F.H.S., Western, A.W., Briggs, P.R., 2004. A rational function approach for estimating mean annual evapotranspiration. Water Resour. 1265 Res. 40, W02502. https://doi.org/10.1029/2003WR002710 Zhang, L., Potter, N.J., Zhang, Y., 2010. Water balance modeling over variable time scales based on the Budyko framework - Model development and testing (vol 360, pg 117, 2008). J. Hydrol. 390, 121–122. https://doi.org/10.1016/j.jhydrol.2010.05.027 Zhang, L., Su, F., Yang, D., Hao, Z., Tong, K., 2013. Discharge regime and simulation for the 1270 upstream of major rivers over Tibetan Plateau. J. Geophys. Res.-Atmos. 118, 8500-8518. https://doi.org/10.1002/jgrd.50665 Zhang, S., Yang, H., Yang, D., Jayawardena, A.W., 2016. Quantifying the effect of vegetation change on the regional water balance within the Budyko framework. Geophysical Research Letters 43, 1140-1148. https://doi.org/10.1002/2015GL066952 1275 Zhang, X., Dong, Q., Zhang, Q., Yu, Y., 2020. A unified framework of water balance models for monthly, annual, and mean annual timescales. J. Hydrol. 589, 125186. https://doi.org/10.1016/j.jhydrol.2020.125186 Zhang, Y., Enomoto, H., Ohata, T., Kitabata, H., Kadota, T., Hirabayashi, Y., 2017. Glacier mass balance and its potential impacts in the Altai Mountains over the period 1990-2011. 1280 J. Hydrol. 553, 662–677. https://doi.org/10.1016/j.jhydrol.2017.08.026 Zhang, Y., Liu, S., Ding, Y., 2006. Spatial variation of degree-day factors on the observed glaciers in western China. Acta Geographica Sinica 61, 89. Zhang, Y., Liu, S., Wang, X., 2019. A dataset of spatial distribution of degree-day factors for glaciers in High Mountain Asia. China Sci. 4, 141–151. Data

https://doi.org/10.11922/csdata.2019.0009.zh

1285

Formatted: Indent: Left: 0 cm, Hanging: 2 ch, First line: -2 ch

Supplementary material for

Altitudinal variation in impacts of snow cover, reservoirs and precipitation seasonality on monthly runoff in Tibetan Plateau catchments

 $Nan\;Wu^{a,b,c,f},\;Ke\;Zhang^{a,b,c,d,e,*},\;Amir\;Naghibi^f,\;Hossein\;Hashemi^f,\;Zhongrui\;Ning^{b,c},\;Jerker\;Jarsj\ddot{o}^g$

^aThe National Key Laboratory of Water Disaster Prevention, Hohai University, Nanjing, Jiangsu, 210024, China

^bYangtze Institute for Conservation and Development, Hohai University, Nanjing, Jiangsu, 210024, China

^cCollege of Hydrology and Water Resources, Hohai University, Nanjing, Jiangsu, 210024, China

^dChina Meteorological Administration Hydro-Meteorology Key Laboratory, Hohai University, Nanjing,

10 Jiangsu, 210024, China

15

^eKey Laboratory of Water Big Data Technology of Ministry of Water Resources, Hohai University, Nanjing, Jiangsu, 210024, China

^fDivision of Water Resources Engineering, LTH, Lund University, Lund, 22100, Sweden

^gDepartment of Physical Geography, Stockholm University, Stockholm, 10691, Sweden;

* Corresponding author at: The National Key Laboratory of Water Disaster Prevention, Hohai University,

Nanjing, Jiangsu, 210098, China

E-mail address: kzhang@hhu.edu.cn (Ke Zhang)

The relative proportions of hydrological variables reflect their importance in hydrological processes, as shown in Figure S1. As both $\Delta S'$ and R exhibited negative values (Fig. 3), their absolute values were used in calculating the relative proportions, ensuring the relative proportions of P_r , S_{melt} , $\Delta S'$, R, and E summed up to 1. The proportion of P_r ($\frac{|P_r|}{|P_r| + |S_{melt}| + |\Delta S'| + |R| + |P_r|}$) increased from March to July, peaking at 50%, and decreased from August to November, with relative proportions in January, February, and December all below 6%. On the other hand, the relative proportion of $\Delta S'$ was higher from January to March and from November to February. S_{melt} primarily occurred in March and April, predominantly distributed in the GZ, ZB, DF, YJ, and ZS, with GZ having the highest proportion (44%). The relative proportions of R and E were generally greater than 10%, with the proportion of R being small from March to June, while E was prominent from February to May.

To clearly illustrate the long-term impacts of reduced snowmelt and reservoir construction on the seasonal dynamics of runoff at the outlet stations, Fig. S3 presents long-term time series (1980–2016) of total runoff, snowmelt runoff, and reservoir contributions. It can be observed that snowmelt and reservoirs contributed similarly to the annual runoff; however, reservoirs significantly altered the intra-annual runoff distribution pattern.

Figure Captions

40

50

55

Figure S1. Mean normalized monthly magnitude of the water balance term relative to the magnitude of all water balance terms, expressed as percentage from 0% (left part of grid cells, dark colors) to 100% (right, light).

Figure S2. Contribution box of different factors to R_V in 10 sub-basins, P_r , S_{melt} , $\Delta S'$ and E_θ represent rainfall, snowmelt, water storage change except snow, and potential evapotranspiration, respectively, P_r - S_{melt} , P_r - $\Delta S'$, P_r - E_θ , S_{melt} - $\Delta S'$, S_{melt} - E_θ , and E_θ - $\Delta S'$ represent their covariance.

Figure S3. Time series of observed total runoff (i.e. monthly discharge volume divided by the total catchment area), runoff contribution of reservoir water storage change (calculated as monthly reservoir storage volume divided by total catchment area) and estimated snowmelt runoff (calculated as the monthly snowmelt volume divided by the total catchment area) from 1980 to 2017 for the whole basin.

Figure §4. Relationship between the monthly ratio of water demand to water supply $(E/(P_r+S_{melt}-\Delta S'))$ and monthly ratio of potential water demand to water supply $(E_0/(P_r+S_{melt}-\Delta S'))$ in the representative basin (LN, YJ and ZS).

Figure S5. Time series of estimated storage change (ΔS) and observed reservoir water storage change ($\Delta S_{Reservoirs}$) from 2002 to 2016 within the nested catchment of TZL.

Table Captions

Table S1. Parameter n values for 10 sub-basins and the annual average evapotranspiration calculated based on the Budyko and extended Budyko framework.

Table 52. The performance of extended Budyko framework in simulating evapotranspiration.

Formatted: Font: Bold

Formatted: Font: Bold

Deleted: S3

Formatted: Line spacing: Double

Formatted: Font: (Default) Times New Roman, 12 pt, Bold

Formatted: Font: (Default) Times New Roman, 12 pt,

Formatted: Font: (Default) Times New Roman, 12 pt

Formatted: Font: (Default) Times New Roman, 12 pt

Formatted: Font: (Default) Times New Roman, 12 pt, Italic, Subscript

Formatted: Font: (Default) Times New Roman, 12 pt

Deleted: ¶

Deleted: Table S2. Location of outlet stations in 10 subbasins and basic hydrological and meteorological information.¶

Deleted: S3

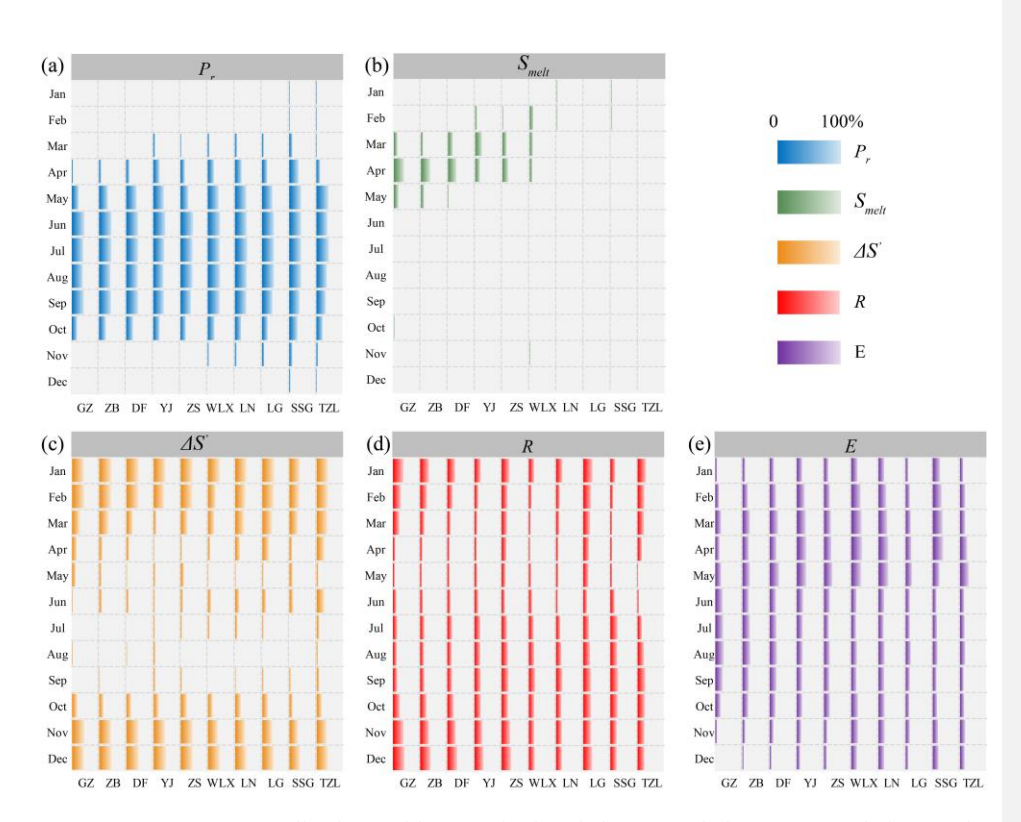


Figure S1. Mean normalized monthly magnitude of the water balance term relative to the magnitude of all water balance terms, expressed as percentage from 0% (left part of grid cells, dark colors) to 100% (right, light).

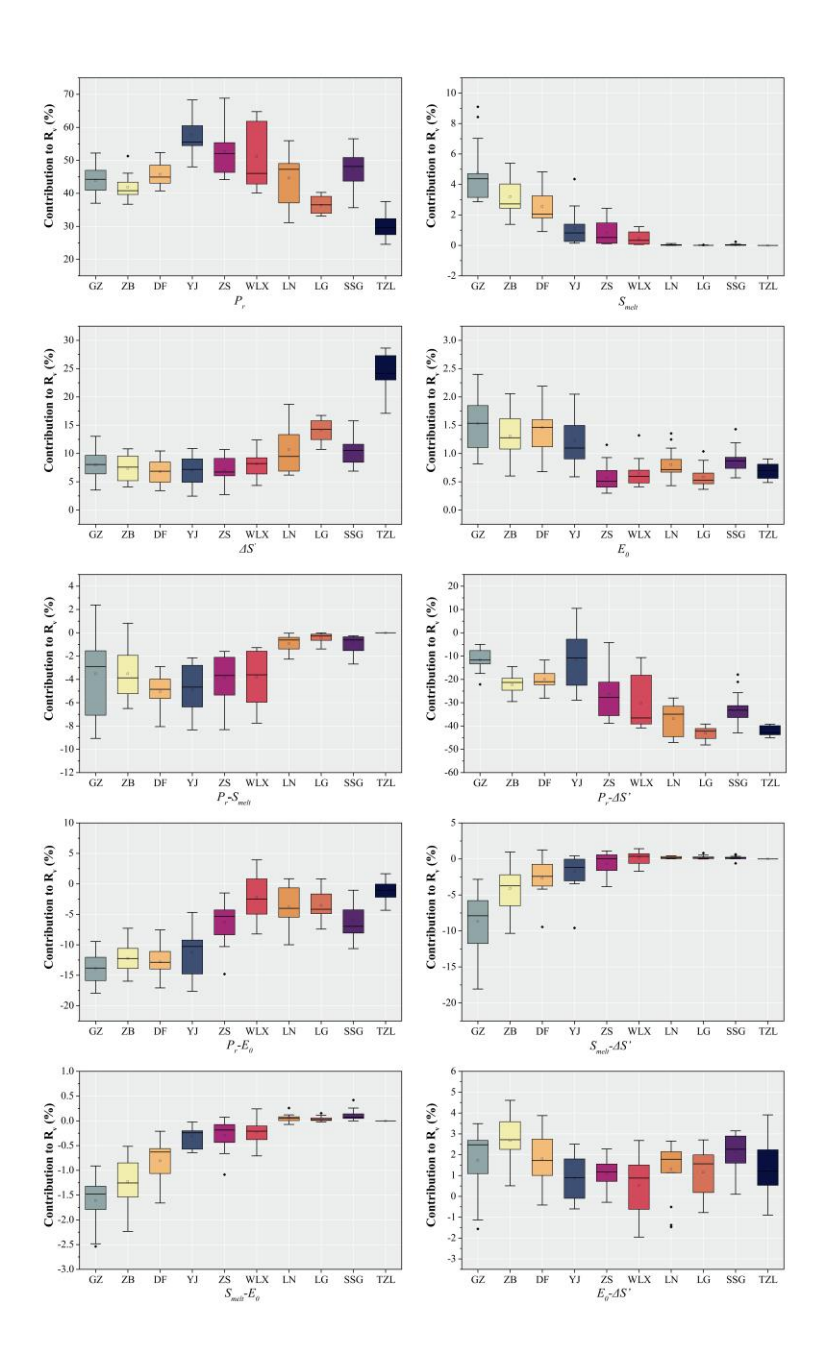


Figure S2. Contribution box of different factors to R_v in 10 sub-basins, P_r , S_{melt} , $\Delta S'$ and E_0 represent rainfall, snowmelt, water storage change except snow, and potential evapotranspiration, respectively. P_r - S_{melt} , P_r - $\Delta S'$, P_r - E_0 , S_{melt} - $\Delta S'$, S_{melt} - E_0 , and E_0 - $\Delta S'$ represent their covariance.

80

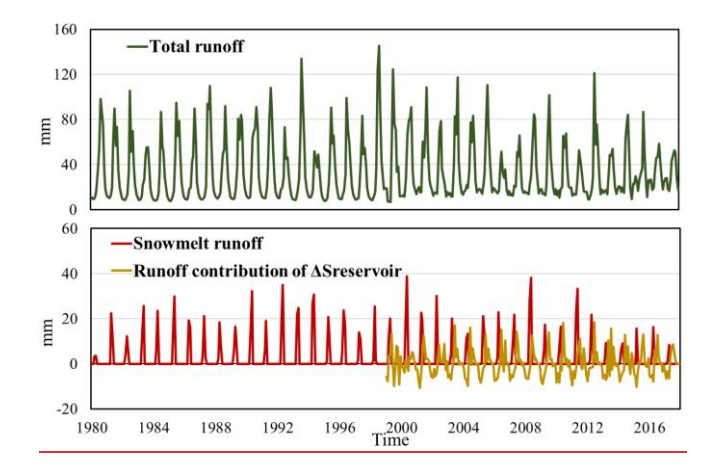


Figure S3. Time series of observed total runoff (i.e. monthly discharge volume divided by the total catchment area), runoff contribution of reservoir water storage change (calculated as monthly reservoir storage volume divided by total catchment area) and estimated snowmelt runoff (calculated as the monthly snowmelt volume divided by the total catchment area) from 1980 to 2017 for the whole basin.

Formatted: Font: Times New Roman, 12 pt

Formatted: Font: Times New Roman, 12 pt

Formatted: Font: Times New Roman, 12 pt, Bold

Formatted: Font: (Default) Times New Roman, 12 pt

Formatted: Line spacing: Double

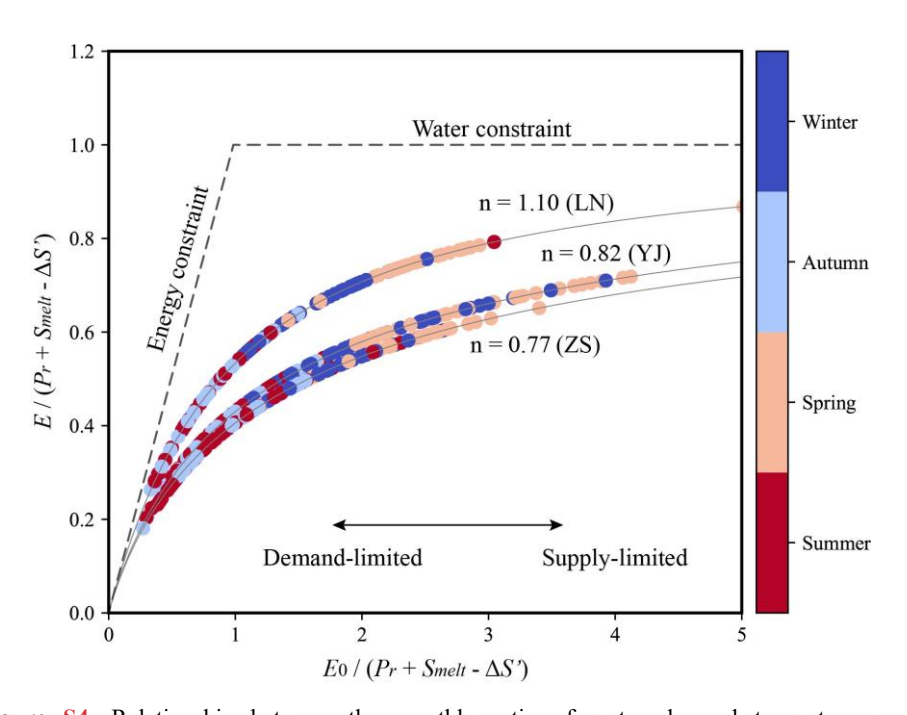
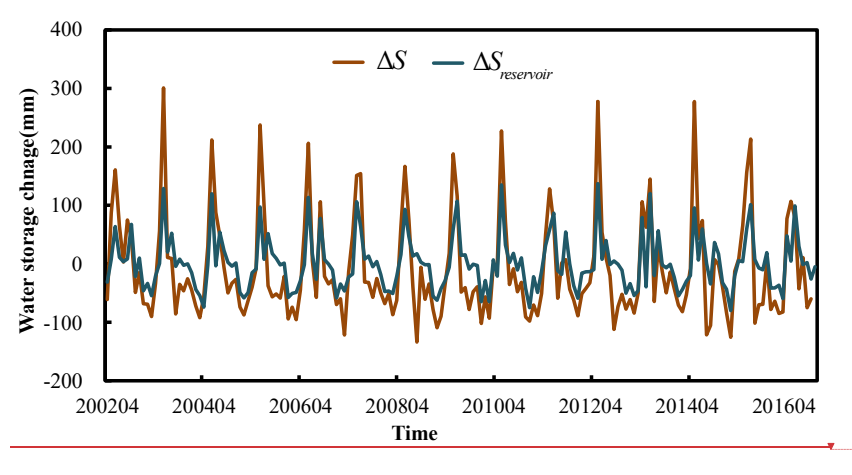


Figure S4. Relationship between the monthly ratio of water demand to water supply $(E/(P_r+S_{melt}-\Delta S'))$ and monthly ratio of potential water demand to water supply $(E_0/(P_r+S_{melt}-\Delta S'))$ in the representative basin (LN, YJ and ZS).



Deleted: S3

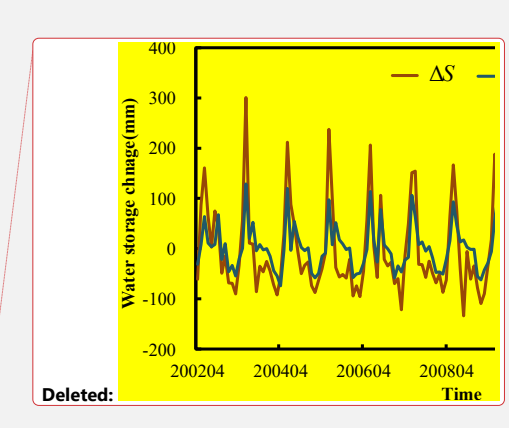


Figure S5_c Time series of estimated storage change (ΔS) and observed reservoir water storage change ($\Delta S_{Reservoirs}$) from 2002 to 2016 within the nested catchment of TZL.

Table S1. Parameter *n* values for 10 sub-basins and the annual average evapotranspiration calculated based on the Budyko and extended Budyko framework.

Basin	<u>GZ</u>	<u>ZB</u>	<u>DF</u>	<u>YJ</u>	ZS	LN	WLX	<u>LG</u>	SSG	TZL	
<u>n</u>	<u>1.26</u>	<u>1.50</u>	<u>1.23</u>	<u>0.82</u>	0.77	<u>1.10</u>	1.68	<u>0.75</u>	<u>0.88</u>	0.79	
<u>E_B</u> (mm)	<u>402</u>	<u>475</u>	<u>455</u>	<u>497</u>	<u>478</u>	<u>527</u>	<u>652</u>	<u>642</u>	<u>604</u>	<u>593</u>	
<u>E_{EB}</u> (mm)	<u>425</u>	<u>479</u>	<u>440</u>	<u>479</u>	<u>442</u>	<u>508</u>	<u>634</u>	<u>706</u>	<u>575</u>	<u>560</u>	•
Table S2. The performance of extended Budyko framework in simulating evapotranspiration.											
Basin	<u>GZ</u>	ZB	DF	YJ	ZS	LN	WLX	LG	SSG	TZL	-
<u>Busin</u>	<u>02</u>	<u> 20</u>	<u> </u>	10	20	271		<u> </u>	<u>550</u>	120	-
NSE	0.87	0.81	0.90	0.93	0.87	0.86	0.93	0.90	0.89	0.82	

Deleted: ¶

Formatted: Font: (Default) Times New Roman, 12 pt

Formatted: Font: (Default) Times New Roman, 12 pt

Formatted: Font: (Default) Times New Roman, 12 pt

Formatted: Font: (Default) Times New Roman, 12 pt,

Not Italic

Formatted: Font: (Default) Times New Roman, 12 pt

Deleted: ¶

Formatted: Indent: First line: 0 cm

95

GZ

Deleted: ¶ GZ

Formatted: Left, Indent: Left: 0 cm, First line: 0 ch, Space Before: 0.5 line, After: 0.5 line